SLAC – PUB – 3911
March 1986
(T/E)

SIGNATURES OF SUPERSYMMETRY IN e^+e^- COLLISIONS*

D. L. BURKE

Stanford Linear Accelerator Center
Stanford University, Stanford, California, 94305

Lecture presented at the SLAC Summer Institute on
Particle Physics, Stanford, California, July 29 – August 9, 1985

* Work supported by the Department of Energy, contract DE – AC03 – 76SF00515.

Signatures of Supersymmetry in e^+e^- Collisions

Over the past dozen years electron-positron collisions have been an extremely fertile source of discovery in elementary particle physics. Signatures of new phenomena are clear and backgrounds are usually quite predictable. To date a number of searches for evidence for supersymmetry in e^+e^- collisions have been made, all with negative results. In these lectures we'll review the techniques used in these searches and examine their results in some detail. Many of these techniques will be directly applicable to future experiments at the SLC and LEP. These new machines may also provide some unique signatures of supersymmetry, and we'll take a look at these possibilities. First we briefly review the general theoretical and experimental features of supersymmetry.

I. Minimal N=1 SUSY

The simplest model of supersymmetry can be summarized with the following postulates – the Black Letter Law[1]:

• Every particle belongs to a supermultiplet that contains equal numbers of fermionic and bosonic degrees of freedom,

$$(S,\ S+1/2) \tag{1a}$$

$$(S,\ S+1/2,\ S+1/2,\ S+1)\ . \tag{1b}$$

For example, a Dirac spinor represents a two-component fermion and its antiparticle, and therefore requires two complex scalar superpartners.

• There is only one (N=1) generator of supersymmetric transformations. This is a raising and lowering spinor operator,

$$Q|\text{fermion}>=|\text{boson}> \tag{2a}$$

$$Q|\text{boson}>=|\text{fermion}> \quad . \tag{2b}$$

In particular, there are no SUSY transformations between left and right-handed fermions, so SUSY models preserve the known V-A weak interactions.

• Supersymmetry implies a multiplicative quantum number R. Known particles are assigned R = +1 and their SUSY partners R = −1. R-parity guarantees that superpartners are produced in pairs, and that the lightest R = ±1 particles are stable.

• Superpartners share all conserved quantum numbers except spin. This important postulate means that all interaction couplings are known.

The particle spectrum that is needed to fulfill this model is given in Table I. Each electroweak eigenstate is matched by a superpartner that differs only in its spin quantum number. In addition, a spontaneously broken theory will contain fermions (Goldstino's $\tilde{G}$) associated with the corresponding super-Higgs mechanism. In supergravity models with locally broken symmetry, the Goldstino can be absorbed by the gravitino to produce a gravitino mass. In either case these models contain a neutral, weakly interacting particle $\tilde{G}$ which might be extremely light.

Note that the mass eigenstates in Table I are not necessarily also weak interaction states. This feature should not be surprising; we already know it from the mixing of the normal weak neutral isoscalar B^0 and the neutral component of the isotriplet W_3^0 to form the mass eigenstates γ and Z^0,

$$\gamma = B^0 \cos\theta_w + W_3^0 \sin\theta_w \tag{3a}$$

$$Z^0 = -B^0 \sin\theta_w + W_3^0 \cos\theta_w \ , \tag{3b}$$

where θ_W is the Weinberg angle. Left and right-handed fermionic states belong to different supermultiplets,

$$(f_L, \tilde{f}_L) \ \text{ and } \ (f_R, \tilde{f}_R) \tag{4}$$

Table I

Minimal SUSY particle spectrum

$R = +1$		$R = -1$	
Weak Eigenstate	Mass Eigenstate	Weak Eigenstate	Mass Eigenstate
$\ell_L^{\pm},\ \ell_R^{\pm}$	$\ell^{\pm}$	$\tilde{\ell}_L,\ \tilde{\ell}_R$	$\tilde{\ell}_L \cos\theta + \tilde{\ell}_R \sin\theta$ $-\tilde{\ell}_L \sin\theta + \tilde{\ell}_R \cos\theta$
ν_L	ν_L	$\tilde{\nu}_L$	$\tilde{\nu}_L$
$q_L^{\pm},\ q_R^{\pm}$	$q^{\pm}$	$\tilde{q}_L,\ \tilde{q}_R$	$\tilde{q}_L \cos\theta + \tilde{q}_R \sin\theta$ $-\tilde{q}_L \sin\theta + \tilde{q}_R \cos\theta$
g	g	$\tilde{g}$	$\tilde{g}$
$W_1,\ W_2,\ H_1,\ H_2$	$W^{\pm},\ h^{\pm}$	$\widetilde{W}_1,\ \widetilde{W}_2,\ \widetilde{H}_1,\ \widetilde{H}_2$	$\widetilde{\chi}_i^{\pm}$ = mixture
$W_3^0,\ B^0,\ H_1^0,\ H_2^0$	$\gamma,\ Z,\ h_1^0,\ h_2^0,\ h_3^0$	$\widetilde{W}_3^0,\ \widetilde{B}^0,\ \widetilde{H}_1^0,\ \widetilde{H}_2^0$	$\widetilde{\chi}_i^0$ = mixture

while the mass eigenstates are generally linear combinations,

$$\tilde{\ell}_1 = \tilde{\ell}_L \cos\theta + \tilde{\ell}_R \sin\theta \tag{5a}$$

$$\tilde{\ell}_2 = -\tilde{\ell}_L \sin\theta + \tilde{\ell}_R \cos\theta \ . \tag{5b}$$

Interactions are governed by $\tilde{\ell}_L$ and $\tilde{\ell}_R$, but detectors see $\tilde{\ell}_1$ and $\tilde{\ell}_2$. For example consider the $\ell\tilde{\ell}\tilde{\gamma}$ vertex shown in Fig. 1. The interaction Lagrangian is given by,

$$\mathcal{L} = \sqrt{2}\, e \left[\bar{\ell} \left(\frac{1+\gamma_5}{2} \right) \tilde{\gamma}\, \tilde{\ell}_L - \bar{\ell} \left(\frac{1-\gamma_5}{2} \right) \tilde{\gamma}\, \tilde{\ell}_R \right] + \text{h.c.} \tag{6}$$

If the mixing angle $\theta = 0$, then $\tilde{\ell}_1 = \tilde{\ell}_L$ and $\tilde{\ell}_2 = \tilde{\ell}_R$, which can lead to rather striking results when these particles are produced in collisions of polarized electrons and positrons. We'll look more closely at this later. If $\theta = 45°$ then Eq. (6) reduces to,

$$\mathcal{L} = \frac{\sqrt{2}}{2} \left[\bar{\ell}\gamma_5 \tilde{\gamma}\, \tilde{\ell}_1 - \bar{\ell}\tilde{\gamma}\, \tilde{\ell}_2 \right] \tag{7}$$

and we see that $\tilde{\ell}_1$ and $\tilde{\ell}_2$ exhibit, respectively, pseudoscalar and scalar interactions.

Mixing in the gauge sector is more complicated. Unlike the R = +1 case in which the spin of the weak bosons W_1, W_2 differs from that of the scalar Higgs particles, the R = −1 charge states $\widetilde{W}_1$, $\widetilde{W}_2$, $\tilde{H}_1$, $\tilde{H}_2$ share common quantum numbers and therefore result in chargino mass states $\tilde{\chi}^{\pm}$ that generally are mixtures of all four weak eigenstates. The neutralino states $\tilde{\chi}^0$ similarly are mixtures of the neutral states $\widetilde{W}_3^0$, $\tilde{B}^0$, $\tilde{H}_1^0$, $\tilde{H}_2^0$. In neither case are the mixing parameters constrained in the simplest theories. The lesson here is that experimental searches for these particles should be defined carefully in terms of the topologies and range of kinematic variables to which they are sensitive. Limits can then be placed on regions of particle masses and mixing angles for particular theoretical models.

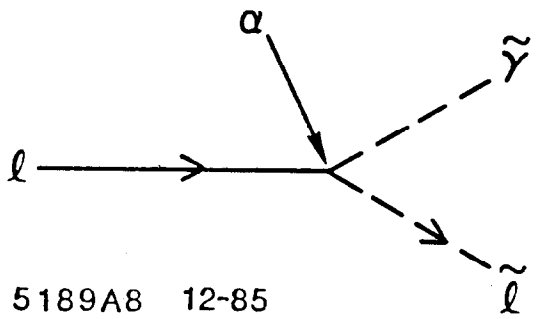

Figure 1. The $\ell\tilde{\ell}\tilde{\gamma}$ electromagnetic vertex.

II. Detecting SUSY

Before beginning detailed discussion of the production of supersymmetric particles by e^+e^- collision, it's useful to summarize what is generally known.

• From e^+e^- experiments it's clear that scalar lepton masses must be larger than $\approx$ 20 GeV almost independently of decay modes or other particle masses, and $>$ 50 GeV if $m_{\tilde{\gamma}}$ is small.

• Scalar quark masses are, perhaps surprisingly, not well constrained. They must be larger than a few GeV since we do not see $q\bar{\tilde{q}}$ or $qq\tilde{q}$ hadronic states.

• Only modest limits from τ-decays exist on scalar neutrino masses.

• Limits on gaugino masses are complicated and extremely dependent upon detailed assumptions or upon masses of other R $= -1$ particles. Gluinos $\tilde{g}$ have been looked for in beam dump experiments and $\bar{p}p$ annihilation final states. These experiments rule out the possibility that both a gluino with mass less than a few GeV and a light scalar quark exist. Searches in e^+e^- annihilation similarly rule out simultaneous existence of light photinos and scalar electrons.

All searches for supersymmetric particles rely on the fact that the lightest R $=$ -1 particle must be stable. Searches for heavy stable particles in e^+e^- and fixed target experiments have not found any hint of charged supersymmetric particles with masses within the kinematic range of present-day machines. Operationally it's usually assumed that the lightest SUSY particle is neutral. Photinos, scalar neutrinos, and neutral gauginos or Goldstinos may be stable and perhaps not too massive. It's important to see how these particles might behave in a detector. The production of any stable, weakly interacting state $\tilde{\nu}$, $\tilde{\chi}^0$ or $\widetilde{G}$ would result in energy that is unseen by most detectors. Possible electromagnetic interactions of the photino shown in Fig. 2 all involve the internal propagator of what is assumed to be a massive charged particle, either a scalar electron or quark. For example, the cross section for the interaction of the $\tilde{\gamma}$ with a quark is approximately (for

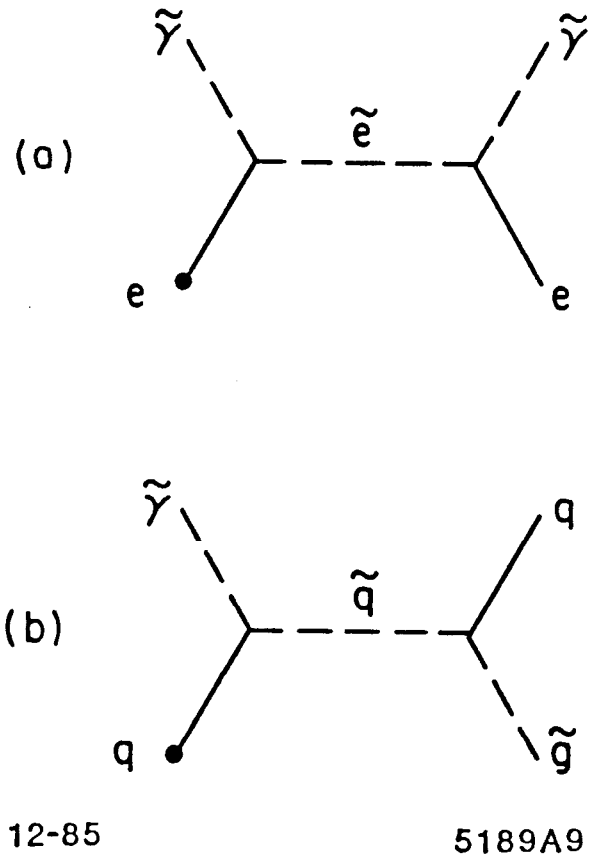

Figure 2. (a) Compton scattering of photinos. (b) Photino hadronic interaction in matter.

$m_{\tilde{q}} \gtrsim m_W$),[2]

$$\sigma_{had}^{\tilde{\gamma}} \approx 2 \cdot 10^{-37} E_{\tilde{\gamma}} \left(\frac{m_W}{m_{\tilde{q}}}\right)^4 F(m_{\tilde{\gamma}},\ E_{\tilde{\gamma}})\ \text{cm}^{-2}\ , \tag{8}$$

where the structure function $F(m_{\tilde{\gamma}},\ E_{\tilde{\gamma}})$ is $\approx 0.1 - 0.2$. This cross section is similar in magnitude to a standard weak interaction. The conclusion is that if the lightest SUSY particle is neutral, then its production, either directly or in the decay chain of a more massive particle, will result in energy and momentum that is not visible to most detectors. It's this missing momentum that becomes the signal of new phenomena. Listed in Table II are probable decay chains for particles in the minimal SUSY model.[3] The circled decay products are likely to be undetectable. Notice that, except for a few special cases corresponding to nearly degenerate mass combinations, the lifetimes of these particles are all quite short. They will probably not be seen as long-lived particles in high resolution vertex detectors.

III. Searches for SUSY at Present-Day e^+e^- Storage Rings

A. Scalar Leptons

Scalar leptons can be pair produced by e^+e^- annihilation through the s-channel neutral current as in Fig. 3a, or in the case of the scalar electron, by the t-channel exchange diagram shown in Fig. 3b. For unpolarized initial electrons and positrons, the superpartners of the left and right-handed leptons, $\tilde{\ell}_L$ and $\tilde{\ell}_R$, are produced with cross sections that depend upon the masses $m_{\tilde{\ell}_L}$ and $m_{\tilde{\ell}_R}$, and in the case of the $\tilde{e}$ on the mass of the neutralino $\tilde{\chi}^0$ exchanged in the t-channel diagram. At the energies of PEP and PETRA we can ignore the contributions of the Z^0 in Fig. 3a, and if we assume that the mass of the $\tilde{Z}^0$ is also large, then the scalar lepton pair-production cross section is,[4]

$$\frac{d\sigma(e^+e^- \to \ell_{\tilde{R}}^+ \ell_{\tilde{R}}^-)}{d\cos\theta} = \frac{\pi\alpha^2\beta^3 \sin^2\theta}{8s} \left[1 + \left(1 - \frac{4K}{1 - 2\beta\cos\theta + \beta^2 + \mu^2}\right)^2\right] \tag{9}$$

Table II

Decay chains and lifetimes of supersymmetric particles

Particle	Decay	Approx. Lifetime (sec)
$\tilde{\ell}$	$\ell + \widetilde{\gamma}$	$2 \times 10^{-22} \ \frac{m_{\tilde{\ell}}^3}{(m_{\tilde{\ell}}^2 - m_{\tilde{\gamma}}^2)^2}$
	$\ell + \widetilde{G}$	$7 \times 10^{-16} \ \left(\frac{\Lambda_{SUSY}}{M_W}\right)^4 \ \frac{1}{m_{\tilde{\ell}}^5}$
$\tilde{\gamma}$	$\gamma + \widetilde{G}$	$7 \times 10^{-16} \ \left(\frac{\Lambda_{SUSY}}{M_W}\right)^4 \ \frac{1}{m_{\tilde{\gamma}}^5}$
$\tilde{q}$	$q + \tilde{g}$ $\hookrightarrow q\bar{q} \ \widetilde{\gamma}$	$2 \times 10^{-23} \ \frac{m_{\tilde{q}}^3}{(m_{\tilde{q}}^2 - m_{\tilde{g}}^2)^2}$
$\tilde{g}$	$q + \bar{q} + \widetilde{\gamma}$	$10^{-11} \ \left(\frac{m_{\tilde{q}}}{M_W}\right)^4 \ \frac{1}{m_{\tilde{g}}^5}$
$\tilde{\nu}$	$\nu + \widetilde{\gamma}$	$10^{-16} \ \frac{1}{M_{\tilde{\nu}}}$
$\widetilde{W}$, $\widetilde{Z}$	typical electroweak decays	

$\bigcirc \longrightarrow$ UNSEEN

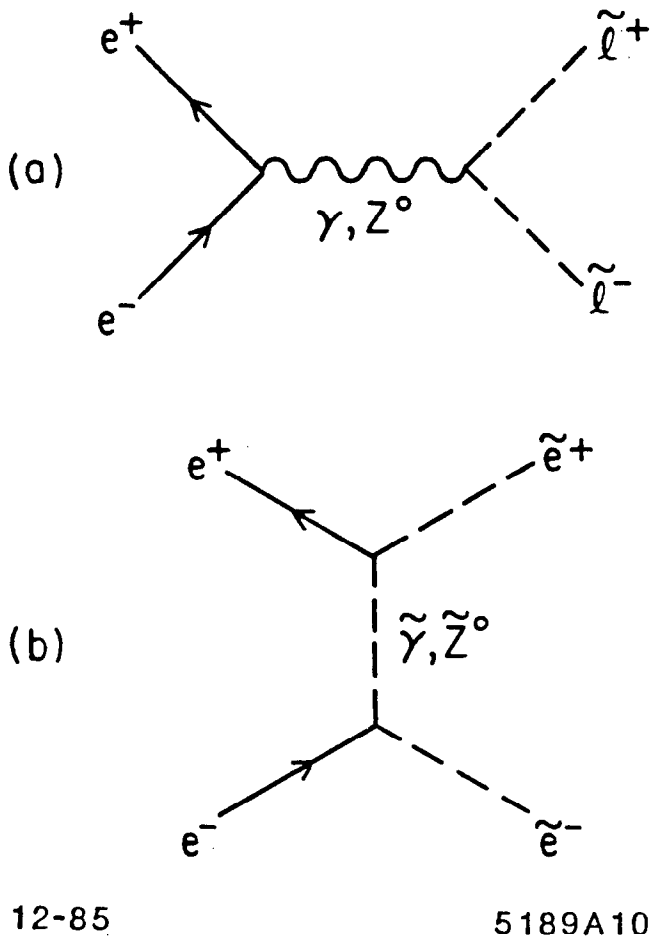

Figure 3. Pair production of scalar lepton pairs in e^+e^- annihilation.

where $\beta = (1 - 4m^2_{\tilde{\ell}_R}/s)^{\frac{1}{2}}$ is the velocity of the $\ell_{\tilde{R}}$, and $\mu^2 = (m_{\tilde{\gamma}}/E_b)^2$, and

$$K = \begin{pmatrix} 0 & \text{for } \ell \neq e \\ 1 & \text{for } \ell = e \end{pmatrix} \quad .$$

The leading term is due to the s-channel diagram (Fig. 3a) and exhibits the β^3 threshold factor and $\sin^2\theta$ angular distribution characteristic of scalar pairs produced by e^+e^- annihilation. When integrated over polar angle this leads to a total cross section (normalized to $e^+e^- \to \mu^+\mu^-$) of $R = 1/4\,\beta^3$. Most experiments are done with unpolarized electron beams and therefore have no control over the separate production rates for $\tilde{\ell}_R$ and $\tilde{\ell}_L$. There are two limiting possibilities for the mass eigenstates $\tilde{\ell}_1$ and $\tilde{\ell}_2$ (Eq. 5) that are of practical experimental interest. The absence of a signal in a search can be interpreted as a limit on the production cross section for the lighter mass state (i.e. if $m_{\tilde{\ell}_1} >> m_{\tilde{\ell}_2}$), or on the production of degenerate states ($m_{\tilde{\ell}_1} = m_{\tilde{\ell}_2}$). These two cases correspond to a factor of two in the expected signal.

Whether the $\tilde{\ell}^{\pm}$ is stable or not, the pair production process leaves an extremely clear signature. Production of stable $\tilde{\ell}^{\pm}$ pairs will result in apparent deviations from the known QED production of lepton pairs, and the $\tilde{\ell}^{\pm}$ may also be seen as new massive charged particles by time-of-flight and/or ionization measurements. Studies of lepton pair production at PEP and PETRA agree with QED to within 2–3%, and several searches for anomalously heavy charged particles in e^+e^- final states are all negative.[5] These clearly rule out the existence of stable $\tilde{e}$, $\tilde{\mu}$, and $\tilde{\tau}$ particles with masses within the kinematic range of these machines.

Possible decay modes of scalar leptons are shown in Fig. 4a. If $m_{\tilde{\ell}} > m_{\ell}$, then the electromagnetic decay $\tilde{\ell} \to \ell\tilde{\gamma}$ will dominate, but in any case, the lifetime of the $\tilde{\ell}$ is expected to be very short (Table II), and the production of $\tilde{\ell}^{\pm}$ pairs will result in a pair of acoplanar leptons as shown in Fig. 4b. Two examples[6] of searches for this signature are shown in Fig. 5. Both the e^+e^- and $\mu^+\mu^-$

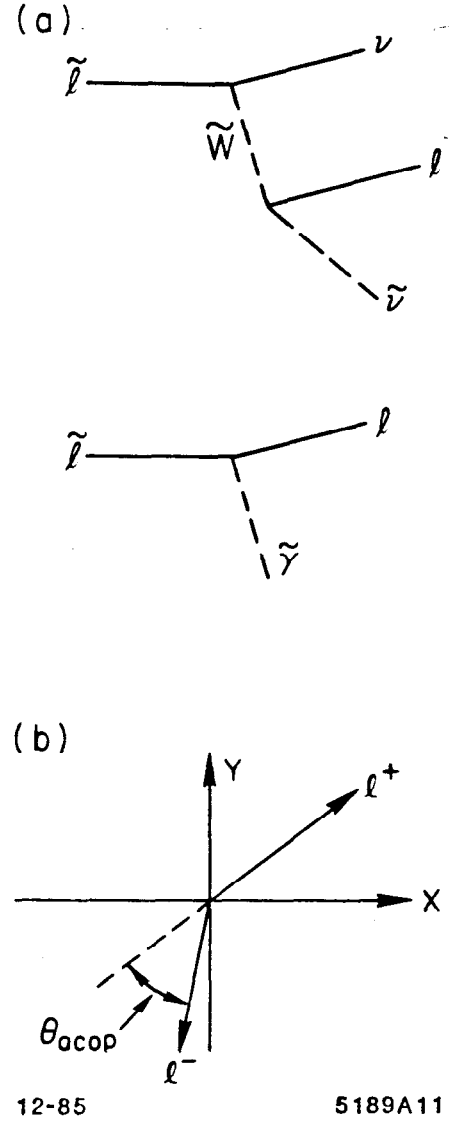

Figure 4. (a) Scalar lepton decays. (b) Definition of acoplanarity.

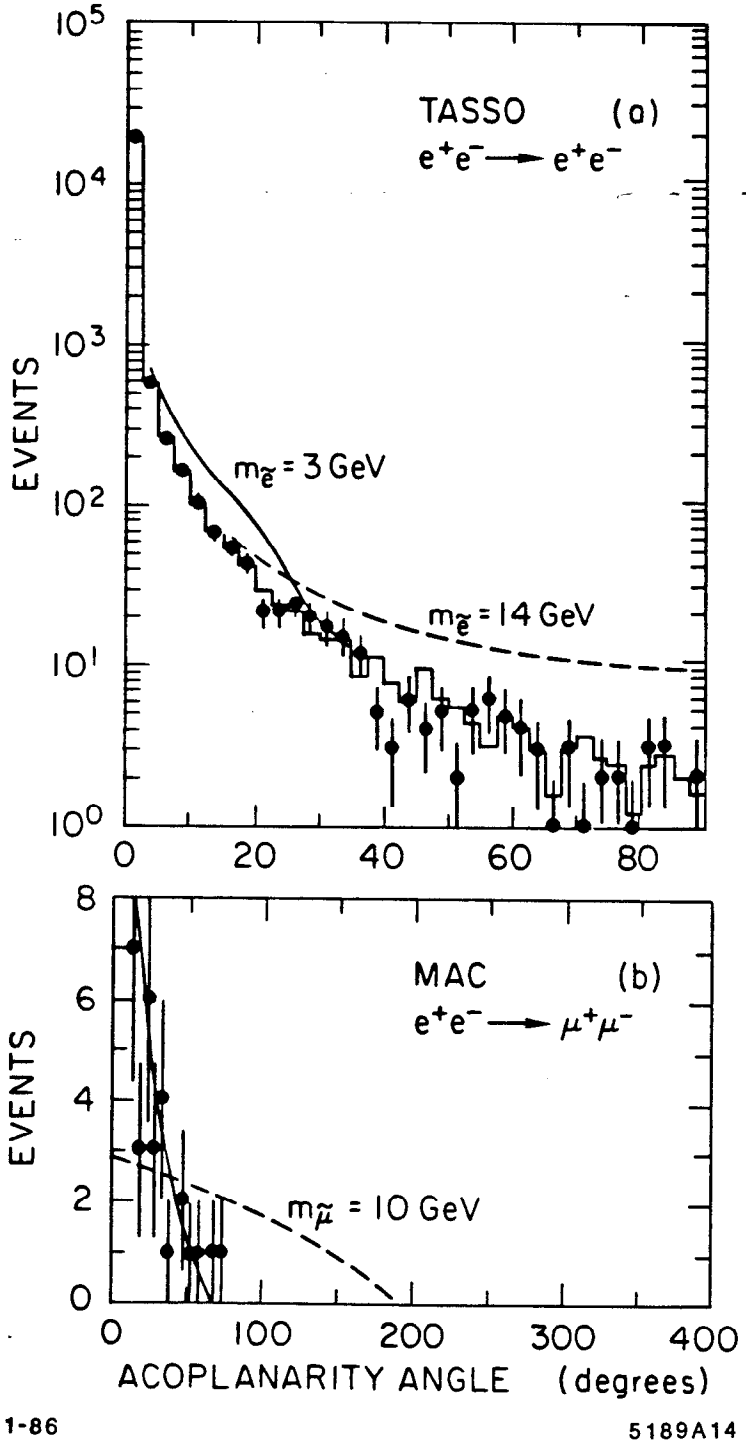

Figure 5. Acoplanarity distribution of (a) electron pairs, (b) muon pairs produced in e^+e^- collision. Anticipated signals are also shown.

final states have a background at large acoplanarity angles due to two-photon processes $e^+e^- \rightarrow e^+e^-\ell^+\ell^-$ in which the outgoing beam electrons remain close to the beam line. The data are completely consistent with these sources and rule out the possible existence of unstable $\tilde{e}$ and $\tilde{\mu}$ with masses $\lesssim 20$ GeV/c^2. A set of limits given by the JADE Collaboration[7] is shown in Fig. 6a. It's assumed that if $m_{\tilde{\gamma}} > m_{\tilde{\mu}}$, then the $\tilde{\mu}$ will be stable, otherwise it decays into $\mu\tilde{\gamma}$. If the mass of the photino is less than, but nearly equal to the mass of the $\tilde{\mu}$, then the muon from the $\tilde{\mu} \rightarrow \mu\tilde{\gamma}$ decay becomes too soft to detect, so a narrow band at $m_{\tilde{\gamma}} \lesssim m_{\tilde{\mu}}$ is not excluded by these searches.

Limits on the mass of the scalar tau $\tilde{\tau}$ are slightly less stringent because the τ itself decays essentially always to either one or three prongs. The mass of the τ is small compared with the beam energy, however, so the decay products follow closely along the direction of flight of the parent. An example of an $e^+e^- \rightarrow \tau^+\tau^-$ event as seen in the Mark II detector is shown in Fig. 7. Detailed studies of the τ-pair production rate and acoplanarity distribution lead to limits on the $\tilde{\tau}$ mass. The best value of 17 GeV is given by the Mark J group.[8] See Fig. 6b.

All of the searches for scalar leptons discussed so far are limited by the available energy of present machines and not by statistics. As a result these limits are not very sensitive to parameters that change the production cross sections such as the mass mixing angle (Eq. 5). For example, the best of these limits on the selectron mass is 23 GeV if the two mass eigenstates are degenerate, and 22 GeV if one is much larger than the other.

It is possible to produce a single scalar electon in e^+e^- collisions by the two diagrams shown in Fig. 8.

$$e^+e^- \rightarrow e\tilde{e}\tilde{\gamma} \tag{10}$$

The Q^2 of the photon in either of these diagrams tends to be small, and the recoil angle given by $Q^2 \approx E^2\theta^2$ is also small. The outgoing beam particle from most events of this type would not be detected, and the signal from such an event

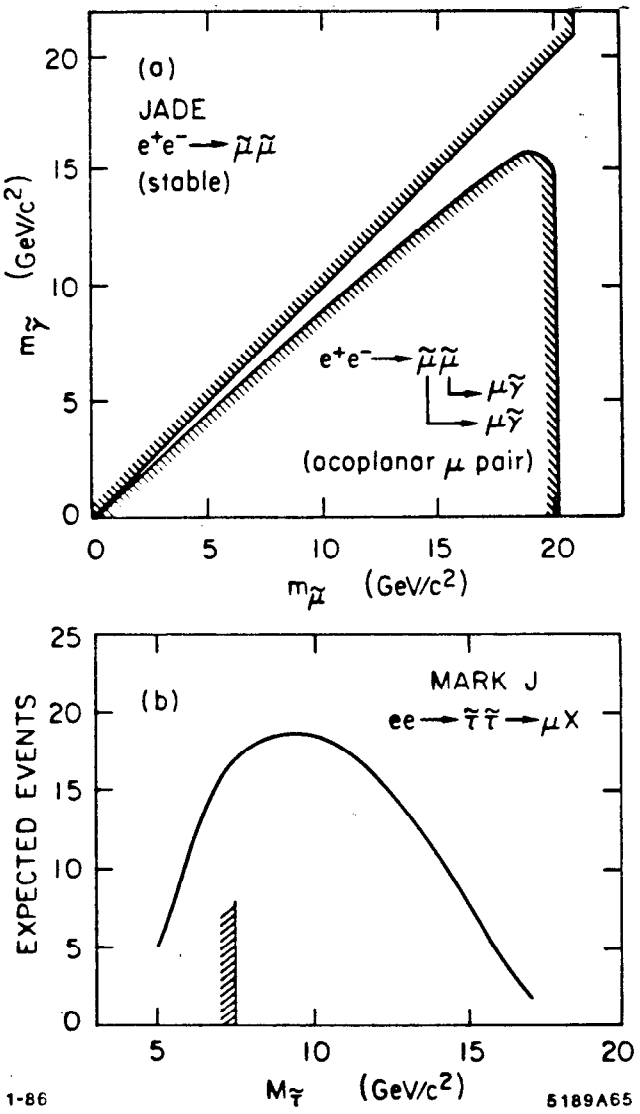

Figure 6. (a) Limits on scalar muon mass. (b) Search for scalar tau events. No events were observed placing a limit at 17 GeV/c^2. Cross hatch is the limit from τ-pair production rate.

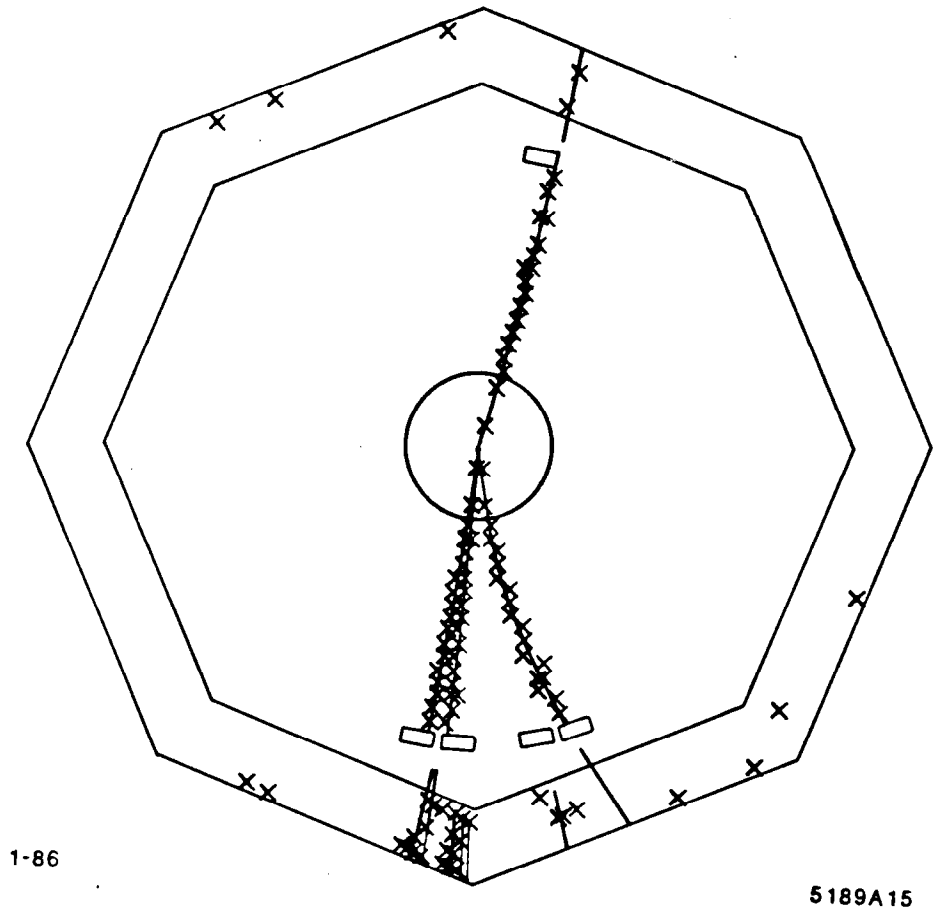

Figure 7. The $e^+e^- \rightarrow \tau^+\tau^-$ as observed in the MARK II detector.

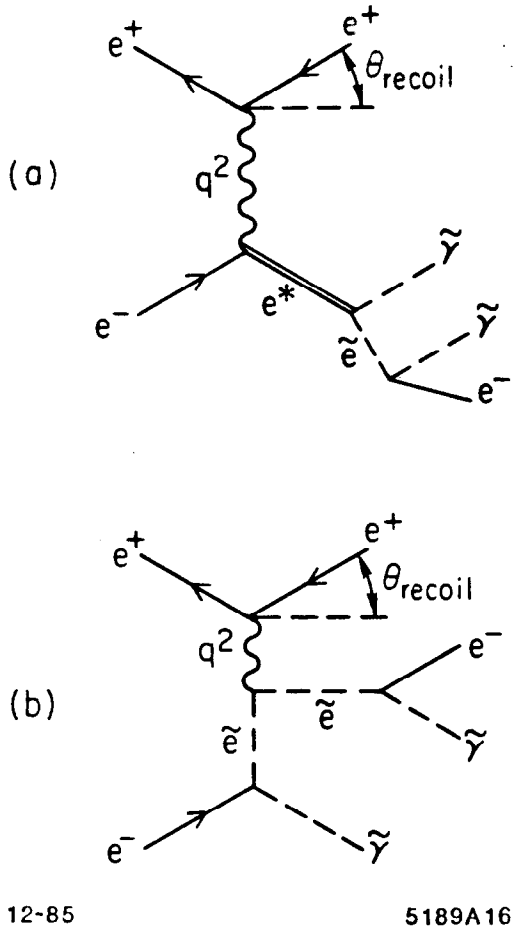

Figure 8. Single $\tilde{e}$ production.

would then be a single isolated electron or positron with significant momentum transverse to the beam. The observable cross section is not small and extends to selectron masses that are larger than the beam energy. For example, the calculated cross section within the acceptance of a search made by the Mark II group,[9] shown in Fig. 9, indicates that with accumulated luminosities in excess of 100 pb^{-1}, it is possible to search for a signal produced by scalar electrons with masses that are $\sim$ 30% greater than the beam energy.

Most detectors leave a major background to this signal caused by radiative Bhabha events

$$e^+e^- \rightarrow e^+e^-\gamma \tag{11}$$

when only one of the electrons is seen (Fig. 10). These occur with well-determined kinematics, however, so for a particular search it is possible to define regions of energy and angle which are background free. Shown in Fig. 11 is the result of the Mark II search. As can be seen, there is a large number of events at the lower energies, but there exists a region that corresponds to large momentum transfers in process (11) that is empty of events. The cross section for the production of signal events in this region is just that shown in Fig. 9.

In this case, the sensitivity of the search is determined by statistics, and the limits depend more sharply on possible mixing of the interaction eigenstates. The limits from the Mark II search are shown in Fig. 12 for the two extreme mixing hypotheses. Notice that the experimenters choose to not place limits in the region $m_{\tilde{\gamma}} > m_{\tilde{e}}$. The assumption is that if this were the case, then the selectron would not decay. The best limits on this process come from the JADE Collaboration[10] at PETRA and extend to $m_{\tilde{e}} = 25.2$ GeV/c^2 for the degenerate mass case and $m_{\tilde{\gamma}} = 0$.

B. Photinos

Although SUSY doesn't require that a photino mass eigenstate exist as the

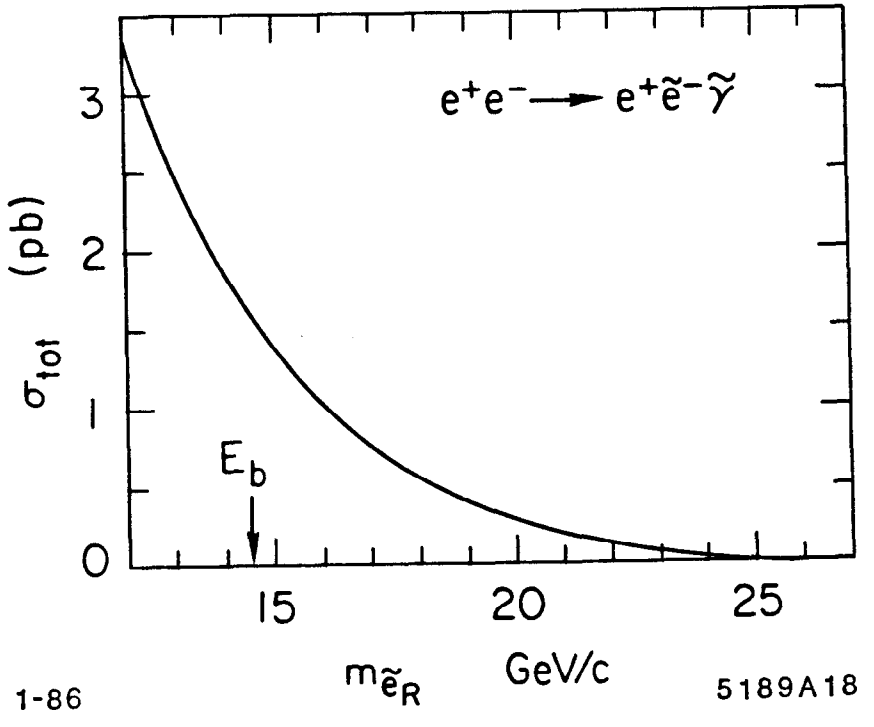

Figure 9. Computed cross section for $e^+e^- \rightarrow e^+\tilde{e}^-\tilde{\gamma}$ within the acceptance of a search by the MARK II group.

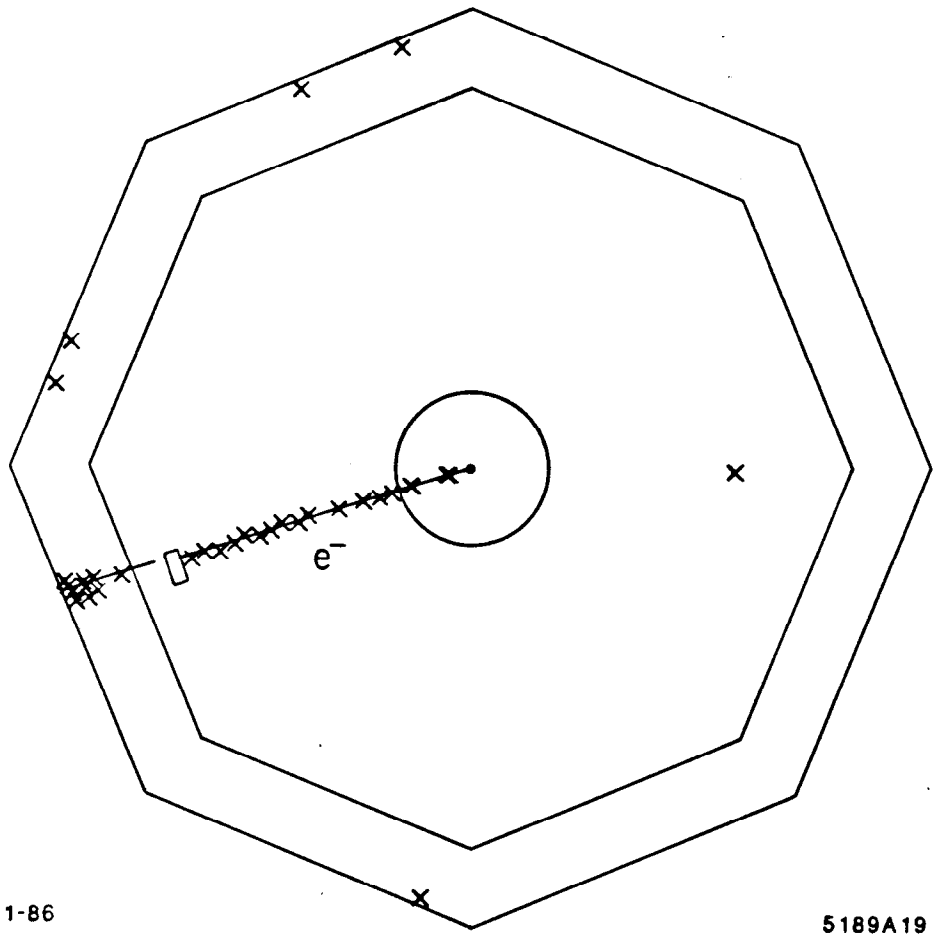

Figure 10. A single electron event in the MARK II.

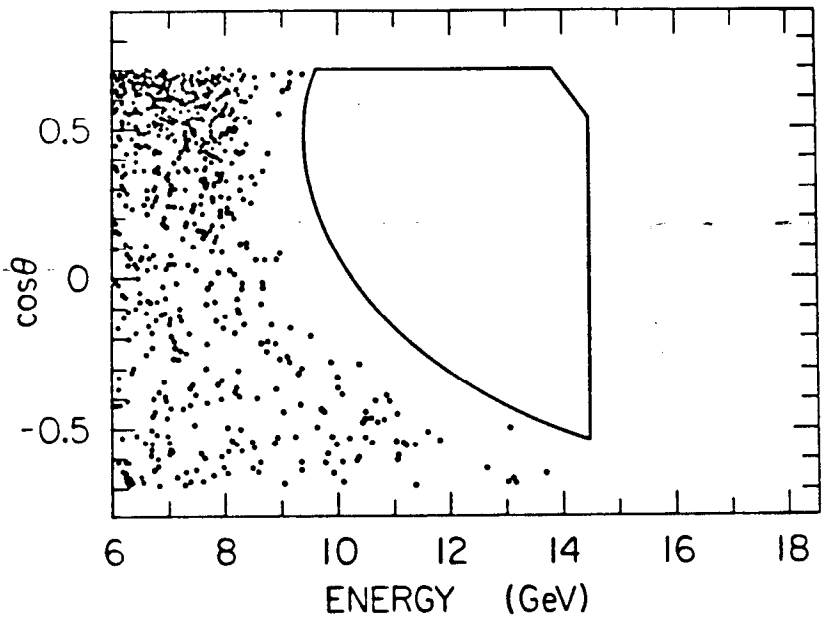

Figure 11. Signal region and observed background from radiative Bhabha scattering in MARK II search for single $\tilde{e}$.

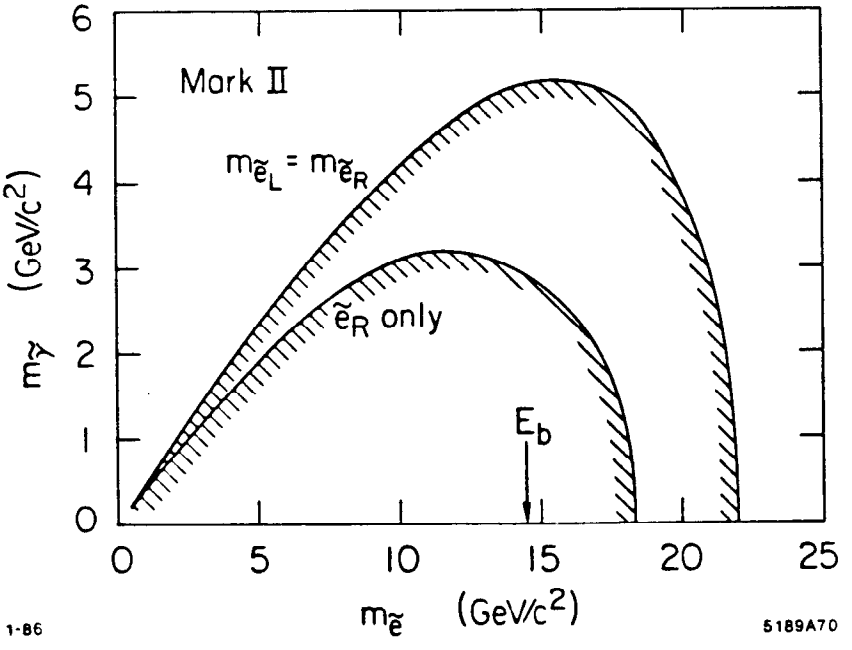

Figure 12. Limits on $\tilde{e}$ mass from single electron search.

particular mixture of neutral gauge bosons,

$$\tilde{\gamma} = \cos\theta_W \, \widetilde{B} + \sin\theta_W \, \widetilde{W}_3^0 \tag{12}$$

it is still important to consider this possibility since it leads to couplings to electrons and positrons that are purely electromagnetic. The pair-production process shown in Fig. 13 occurs with a cross section[11]

$$\frac{d\sigma(e^+e^- \to \tilde{\gamma}\tilde{\gamma})}{d\cos\theta_{\tilde{\gamma}}} = \frac{\pi\alpha^2 s\beta^3}{4\, m_{\tilde{e}_R}^4}(1+\cos\theta_{\tilde{\gamma}}^2) \tag{13}$$

with $\beta = (1-4m_{\tilde{\gamma}}^2/s)^{\frac{1}{2}}$ and the assumption $m_{\tilde{e}_L} >> m_{\tilde{e}_R} >> \sqrt{s}$. The actual propagator is given by

$$\sigma \sim \left(m_{\tilde{e}_R}^{-4} + m_{\tilde{e}_L}^{-4}\right) \tag{14}$$

which reduces to $(1/m_{\tilde{e}_R})^4$ in the limit $m_{\tilde{e}_L} = m_{\tilde{e}_R}$. Notice also that since the photino is a self conjugate (Majorana) fermion, then Fermi statistics require that the photino pair be produced with the β^3 threshold factor of a p-wave process. The cross section (Eq. 13) differs in scale from the pair-production of normal photons only because of the mass of the exchanged selectron. It is large at small $\tilde{e}$ mass, and will become weak, but not unusably small, for $m_{\tilde{e}} \sim m_W$.

If the photino is more massive than the selectron, then the decay $\tilde{\gamma} \to \tilde{e}^+e^-$ is possible, but as we have seen, a selectron of mass within the range of PEP or PETRA has already been ruled out. It's not going to be fruitful to pursue this possibility. A more interesting signature occurs if the Goldstino $\widetilde{G}$ exists either as a particle or as a component of, for example, the gravitino and is lighter than the photino. Then the decay shown in Fig. 14 proceeds with a lifetime (ignoring the mass of the $\widetilde{G}$),[12]

$$\tau_{\tilde{\gamma}} = \frac{8\pi d^2}{m_{\tilde{\gamma}}^5} = 1.7\times 10^{-23}\left(\frac{\Lambda_{SUSY}}{m_{\tilde{\gamma}}}\right)^4\left(\frac{1\text{GeV}}{m_{\tilde{\gamma}}}\right) \quad , \tag{15}$$

where $d = \Lambda_{SUSY}^2$, and Λ_{SUSY} is the mass scale at which supersymmetry is broken. If Λ_{SUSY} is not too large or $m_{\tilde{\gamma}}$ too small, then the pair-production

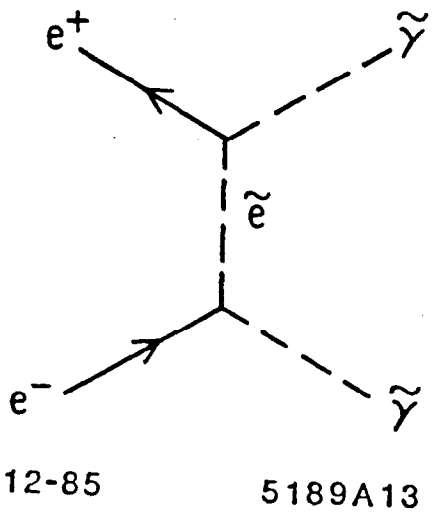

Figure 13. Production of photino pairs by e^+e^- annihilation.

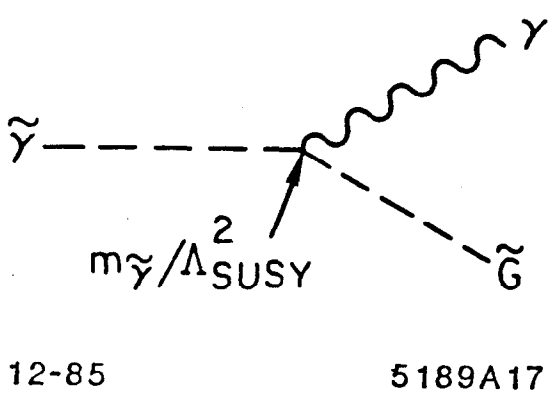

Figure 14. Photino decay.

process (Fig. 13) and subsequent decay of the photinos will result in a pair of photons with missing energy and momentum. A search can be made for acoplanar photon pairs, or alternatively, for colinear photon pairs with energies that are not equal to the beam energy. A photino with a mass greater than $\sim$ 10% of the beam energy will produce a visible signal in the first case, while light photinos will fall into the back-to-back photon sample. The result of such a search[13] at PETRA is shown in Fig. 15. In neither case is there any signal. This experiment is sensitive to a region of $m_{\tilde{\gamma}}$ and d that depends upon $m_{\tilde{e}}$ (Eq. 13); for $m_{\tilde{e}}$ = 40 GeV/c^2 this region is shown in Fig. 16. The upper edge of the region is determined by the beam energy and the lower diagonal edge is determined by the radius of the detector and the photino lifetime (Eq. 15). Also shown in the figure is a bound taken from cosmological arguments; if $m_{\tilde{\gamma}}$ is too small or d too large, then the photino lifetime becomes long, and we would expect a sea of photinos to fill the universe.

Many presently fashionable theories of supersymmetry place $\Lambda_{SUSY} \sim 10^{11}$ GeV, in the so-called "hidden" sector. This would make the photino essentially stable to $\gamma\tilde{G}$ decay. If the mass of any scalar neutrino is less than that of the photino the $\tilde{\gamma}$ might still decay through the "photino β-decay" diagram shown in Fig. 17. The signature would be a final state consisting of four leptons with missing energy and momentum. This would need to be separated from a $\tau^{\pm}$-pair background, and no limits on this possibility have been reported in the literature.

If the photino exists but is stable or long-lived, then it still creates a signature with e^+e^- collisions in which one of the initial state leptons radiates a photon as in Fig. 18. The result is a single isolated photon with no other particles visible in the final state. The cross section for this process is written as a function of the energy E_γ and polar angle θ_γ of the produced photon,[11,14]

$$\frac{d\sigma}{dE_\gamma\, d\cos\theta_\gamma} \approx \frac{\alpha}{\pi} \cdot \frac{1}{E_\gamma \sin^2\theta_\gamma} \cdot \sigma(e^+e^- \rightarrow \tilde{\gamma}\tilde{\gamma}) \quad . \tag{16}$$

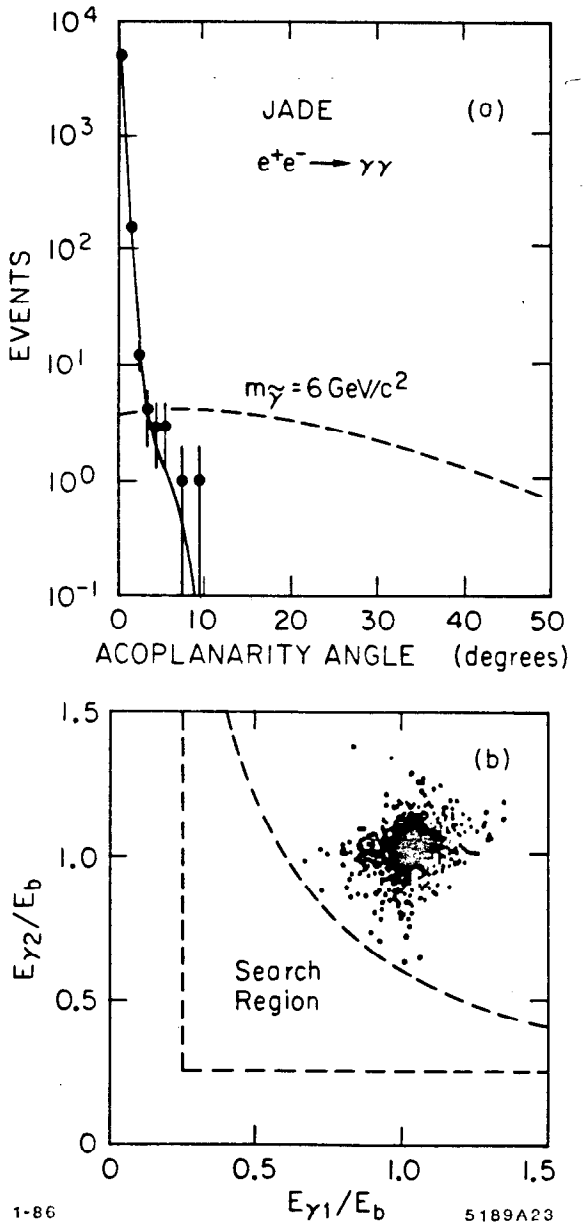

Figure 15. (a) Search for acoplanar photon pairs. (b) Search for colinear photon pairs with missing energy.

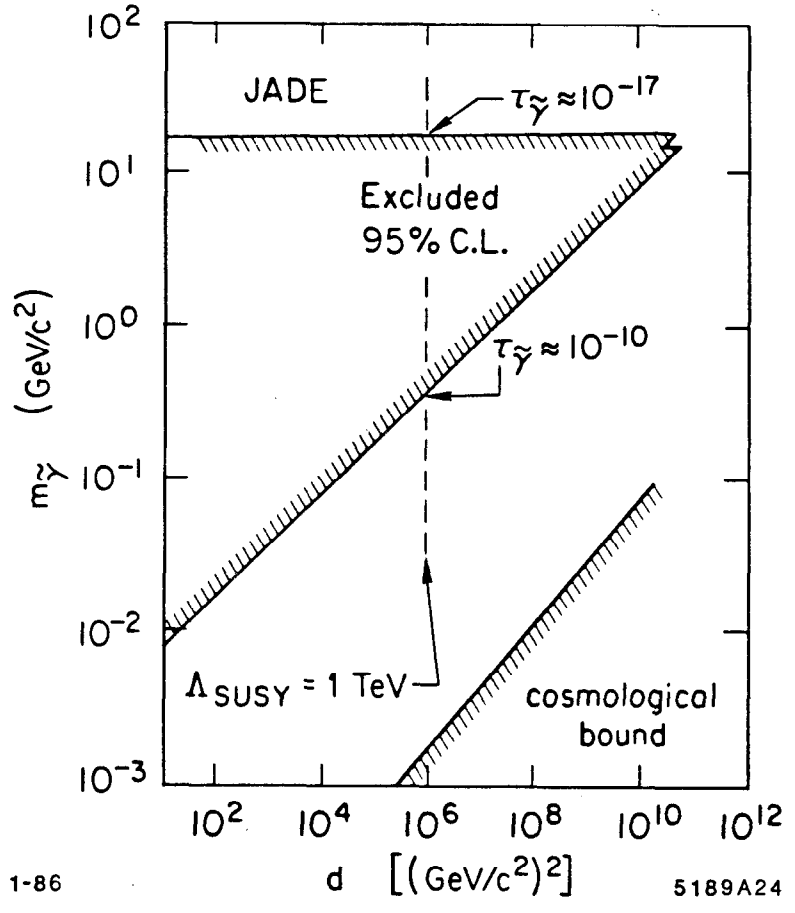

Figure 16. Limits on photino decay.

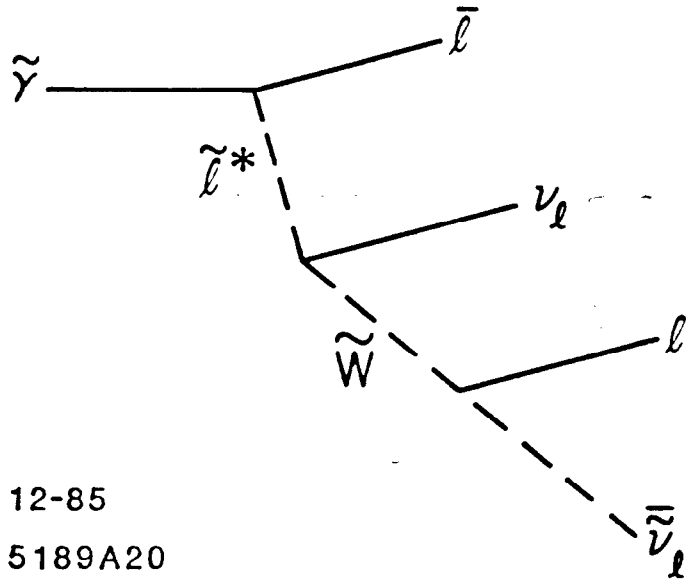

Figure 17. Photino β-decay.

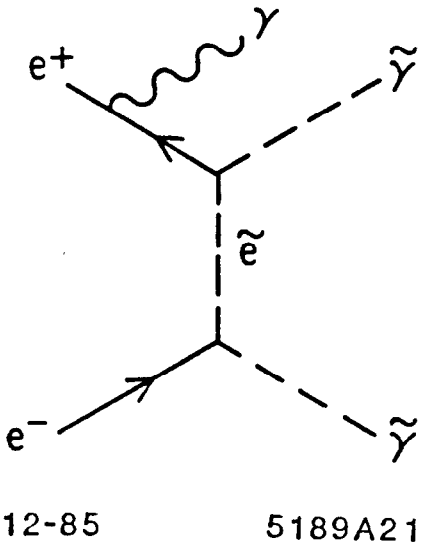

Figure 18. Radiative photino pair production.

For $m_{\tilde{e}_L} >> m_{\tilde{e}_R} >> \sqrt{s}$,

$$\frac{d\sigma}{dE_\gamma d\cos\theta_\gamma} \approx \frac{\alpha^3}{E_\gamma \sin^2\theta_\gamma} \cdot \frac{s}{m_{\tilde{e}_R}^4} \cdot f(E_\gamma, \cos\theta_\gamma) \quad , \tag{17}$$

where $f(E_\gamma, \cos\theta_\gamma)$ is a relatively weak function of E_γ and θ_γ. This cross section leads to a few detected events even for $m_{\tilde{e}_R}$ much larger than the beam energy. A comparison[15] of the cross section with the standard weak interaction process

$$e^+e^- \rightarrow \gamma\nu\bar{\nu} \tag{18}$$

is shown in Fig. 19 for $m_{\tilde{\gamma}} = 1$ GeV and two values of $m_{\tilde{e}_R}$. At machines like PEP and PETRA the production of photino pairs is larger than process (18), and with data samples in excess of 100 pb^{-1} corresponds to observable signal rates of 10 events or so for $m_{\tilde{e}_R}$ as large as 40 GeV. Larger values of $\sqrt{s}$ are less favorable for this particular technique because the weak cross section grows quickly while the $\gamma\tilde{\gamma}\tilde{\gamma}$ process begins to fall as $\sqrt{s}$ exceeds $m_{\tilde{e}_R}$.

The isolation of the $\gamma\tilde{\gamma}\tilde{\gamma}$, or $\gamma\nu\bar{\nu}$, final state from backgrounds is a difficult experimental task. Electronic noise, debris from stray beam particles, and cosmic ray interactions must be eliminated by careful reconstruction and identification of photons. It's particularly important to be able to reconstruct the origin in space and time of single photon candidates. Elimination of backgrounds that might be created by e^+e^- interactions is done by applying kinematic constraints to candidate events. For example, radiative Bhabha scattering (Fig. 20) is potentially the most severe problem, but can be eliminated by requiring that the momentum transverse to the beam line of the detected photon be above a particular minimum value. In that case, at least one other particle must appear above a minimum recoil angle

$$\theta_{recoil}^{min} = \frac{p_{T\gamma}^{min}}{2E_b} \tag{19}$$

to balance momentum. As an example, if we want to cut at $p_{T\gamma}^{min} = 1$ GeV with beam energy $E_b = 14.5$ GeV, then the detector must be sensitive to charged

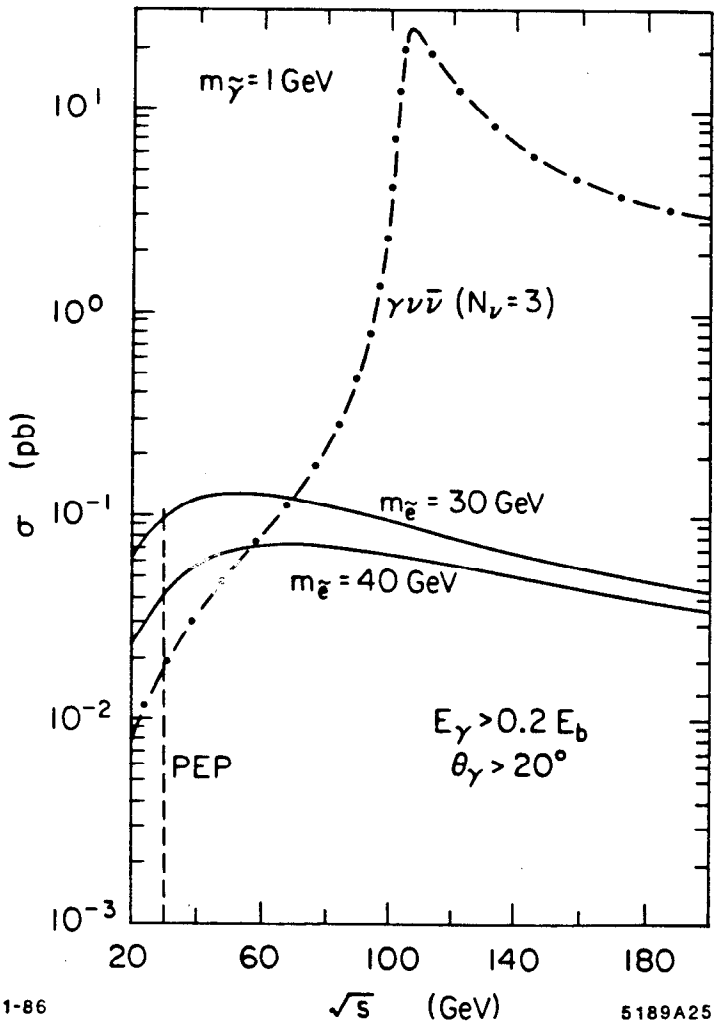

Figure 19. Comparison of cross sections for $\gamma\nu\tilde{\nu}$ and $\gamma\tilde{\gamma}\tilde{\gamma}$. The peak of the $\gamma\nu\bar{\nu}$ cross section is shifted by the requirement $E_\gamma > 0.2E_b$.

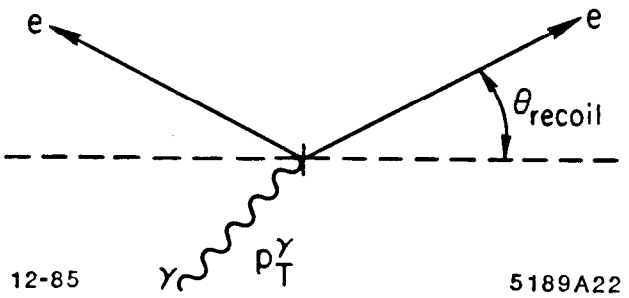

Figure 20. Radiative Bhabha scattering.

particles and photons at all polar angles greater than 30 mr to eliminate backgrounds from normal hadronic, two-photon, and QED processes. It's clear that the search for single-photon events demands a quiet, well-shielded detector with large solid angle coverage. A detailed account of the searches that have been reported is given in another paper in these proceedings.[16] There is no signal in these data above that expected from the standard weak process (18). The best limits placed on $m_{\tilde{\gamma}}$ and $m_{\tilde{e}}$ by all search techniques discussed so far are summarized in Fig. 21.

C. Scalar Quarks

At first thought it might seem that e^+e^- annihilation would be a good place to look for the production of scalar quarks. The signatures left by these particles are not, however, as distinctive as one might hope. The lowest-energy bound state of two scalar particles must be produced in e^+e^- annihilation through a p-wave because the overall spin-parity must be $J^{pc} = 1^{--}$. Unfortunately this means that the leptonic width of this ground state is proportional to the derivative of the wavefunction at the origin,[17]

$$\Gamma_{ee}(\tilde{V} \to e^+e^-) = 24\alpha^2 e\tilde{q}^2 \frac{|R'_p(0)|^2}{m^4_{\tilde{V}}} \quad . \tag{20}$$

This results in estimates of very small production rates. For example, the calculations shown in Fig. 22, made with a potential given by,[17]

$$V(r) = -\frac{k}{r} + \frac{r}{a^2} \tag{21}$$

and parameters k and a^2 taken from fits to the charmonium spectrum, yield leptonic widths that are below the sensitivity of experiments[18] at SPEAR, CESR and DORIS even for the more optimistic choice of a charge = 2/3 scalar quark.

Production of unbound $\tilde{q}\bar{\tilde{q}}$ pairs (Fig. 23) proceeds with a cross section pro-

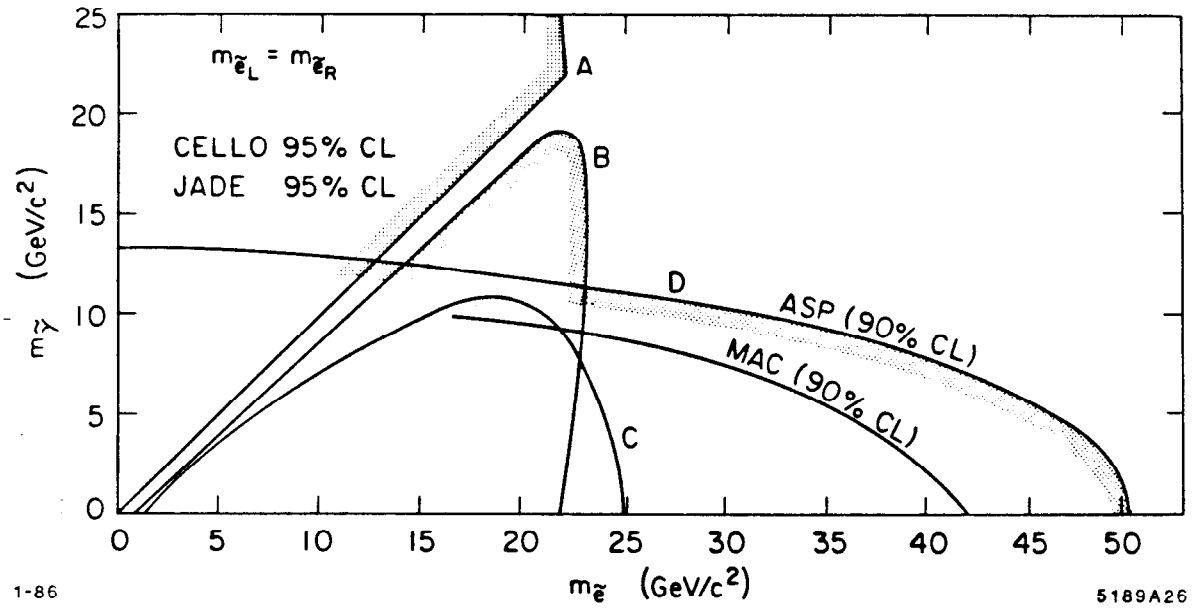

Figure 21. Summary of limits on $m_{\tilde{e}}$ and $m_{\tilde{\gamma}}$. Curve A: stable massive charged particles. Curve B: acoplanar e^+e^- pairs. Curve C: single electron production. Curve D: single photon production.

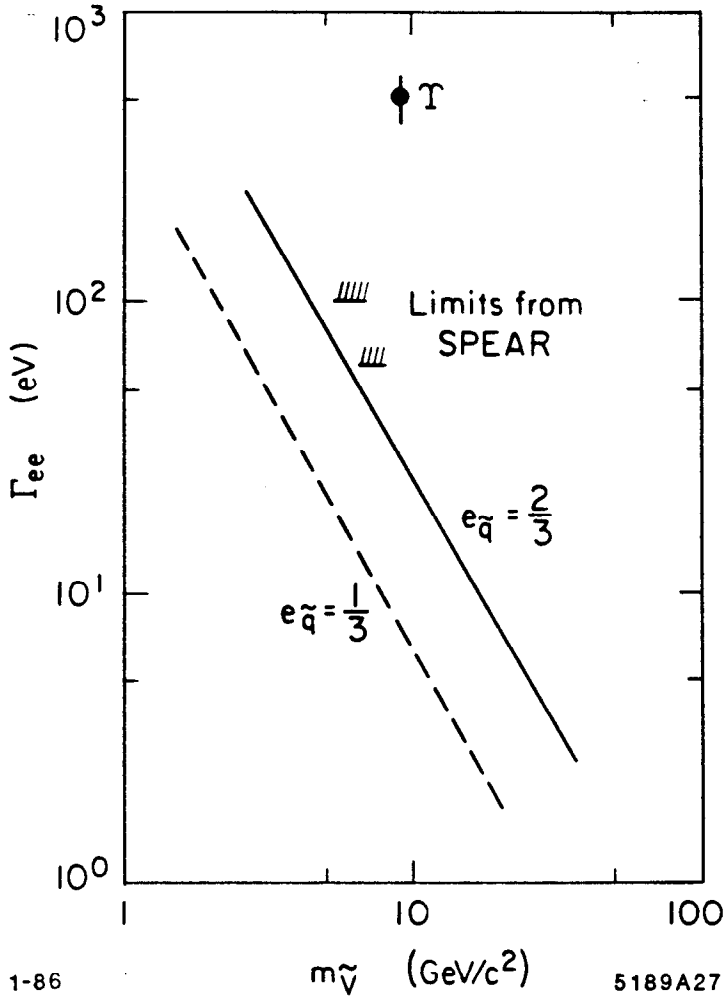

Figure 22. Computed electron partial widths for gluino bound states. Limits from SPEAR and the partial width of the upsilon are also shown.

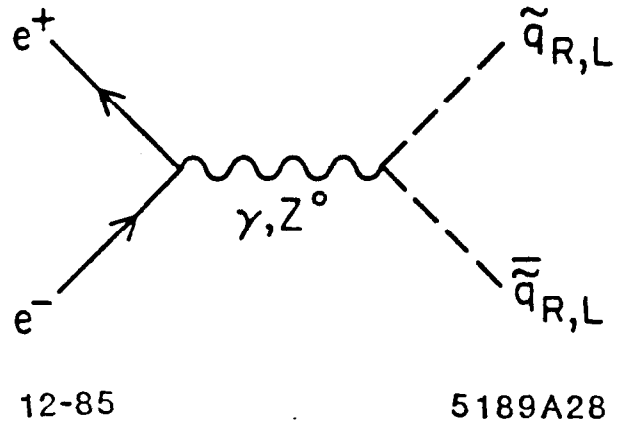

Figure 23. Pair production of scalar quarks.

portional to that for $e^+e^- \to \mu^+\mu^-$

$$R_{\tilde{q}_R} \equiv \sigma(e^+e^- \to \tilde{q}_R\bar{\tilde{q}}_R)/\sigma(e^+e^- \to \mu^+\mu^-) = \frac{3}{4}e_{\tilde{q}}^2\beta^3 \quad , \tag{22}$$

where β is the velocity of the $\tilde{q}$ in the center of mass system. Notice that a light ($\beta \approx 1$) charge 2/3 scalar quark is produced at the same rate as a normal charge 1/3 quark; $R_{\tilde{q}_R} = 0.33$ for $e_{\tilde{q}} = 2/3$ and $\beta = 1$. The threshold factor β^3, shown in Fig. 24, is not negligible for large masses, and hinders the detection of such particles. The best experimental measurements[19] of the total e^+e^- hadronic cross sections are summarized in Table III. At $\sqrt{s} = 34.4$ GeV the data are in agreement with the QCD expectation within the quoted systematic errors, but they are consistently above the QCD value, so the upper limit that they place on any excess is comparable to the signal that would be produced by even a light charged 2/3 $\tilde{q}_R$. No conclusions can be drawn from these numbers.

It's possible that a massive scalar quark would have two-body decay modes as shown in Fig. 25a. Production of $\tilde{q}\bar{\tilde{q}}$ pairs would then lead to a final state that consists of a pair of acoplanar quark jets. An example of a search[20] for events of this type is shown in Fig. 26. Decays of heavy quarks and gaps in the coverage of the detector generate a background of events with acoplanarity angles as large as 45–50 degrees, but the presence of a signal at larger values is clearly ruled out.

While two-body decays of a scalar quark would leave a sharp experimental signature, they are unfortunately not the most likely decay mode of this strongly interacting particle. Decays through the gluino, as in Fig. 25b, will obviously dominate unless prevented by kinematics (e.g. if $m_{\tilde{g}} >> m_{\tilde{q}}$). A search for evidence of these decays can be made by closely examining the shape parameters of hadronic events. If the scalar quark is not too light, then its decay will produce a highly acoplanar spherical event which will be visible against the background of normal two and three-jet QCD events. Fig. 27a defines the triangle diagram used to plot the aplanarity A and sphericity S which are defined in terms of the

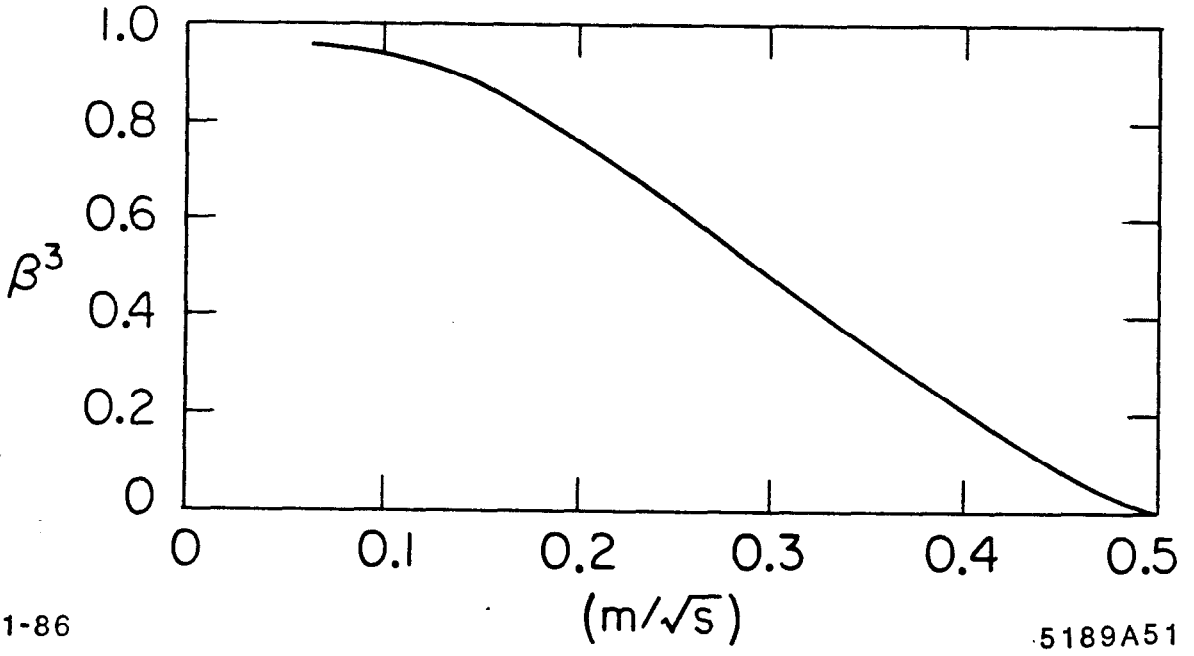

Figure 24. The β^3 threshold factor for production of scalar particles by e^+e^- annihilation.

TABLE III

Summary of R measurements in e^+e^- annihilation and the second order QCD prediction for $\alpha_s = 0.13 \pm 0.02$.

Experiment	$\sqrt{s}$ (GeV)	$R \pm \Delta R_{\rm stat} \pm \Delta R_{\rm sys}$
MAC	29.0	$3.87 \pm 0.10 \pm 0.10$
MARK II	29.0	$3.90 \pm 0.05 \pm 0.25$
JADE	34.4	$3.99 \pm 0.04 \pm 0.10$
MARK J	34.4	$3.95 \pm 0.05 \pm 0.22$
TASSO	34.4	$4.05 \pm 0.05 \pm 0.19$
$O(\alpha_s^2)$ QCD	34.4	3.83 ± 0.03

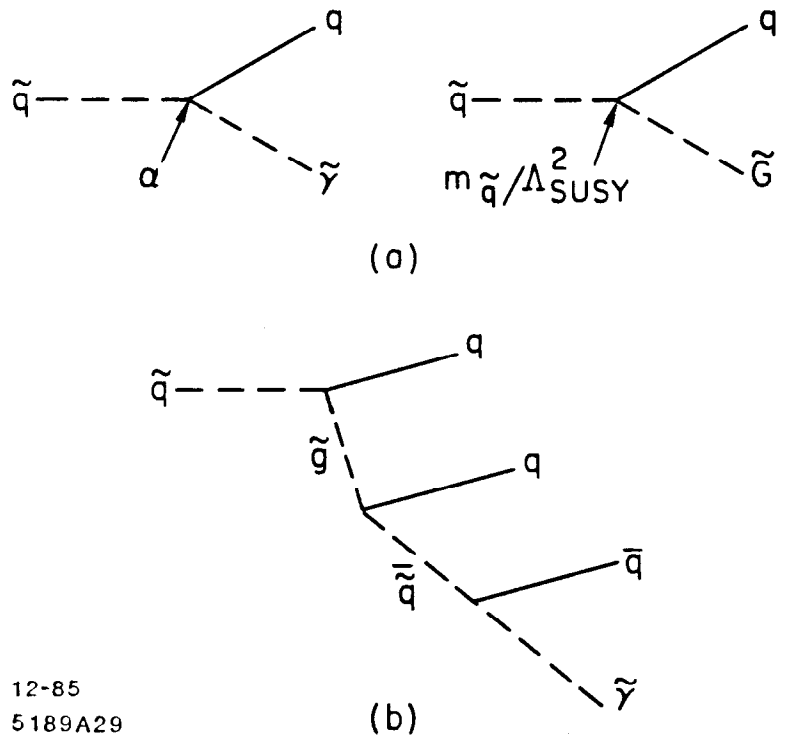

Figure 25. Decays of scalar quarks.

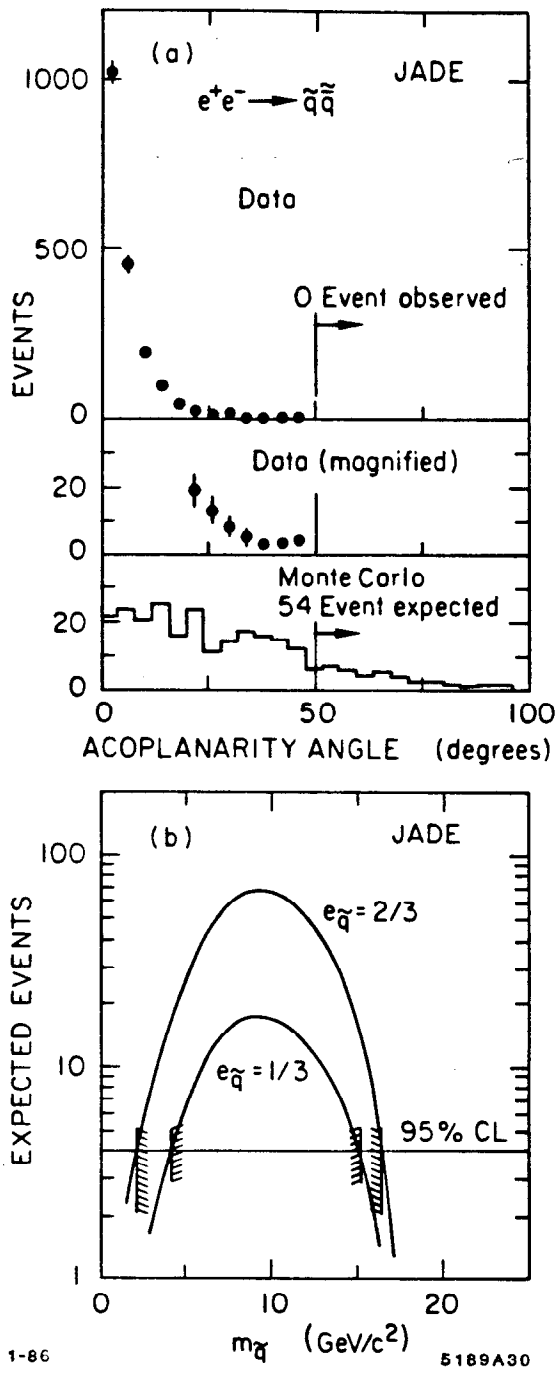

Figure 26. (a) Search for acoplanar jet pairs produced by e^+e^- annihilation. (b) Limits on masses of scalar quark that decays electromagnetically.

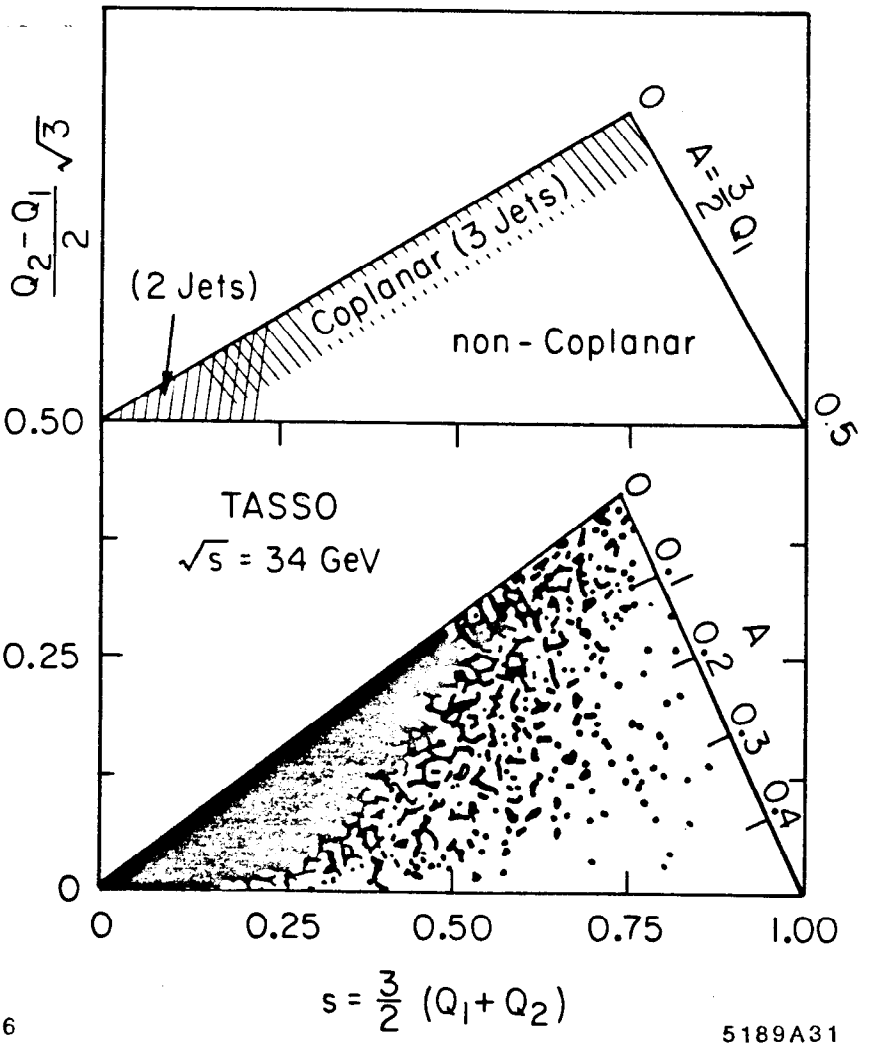

Figure 27. Triangle plot of jet shape parameters sphericity and aplanarity.

normalized eigenvalues Q_i of the momentum tensor,

$$M_{\alpha\beta} = \sum_j p_\alpha^j \, p_\beta^j \quad . \tag{23}$$

The sum runs over all particles in the event. Data taken by the TASSO Collaboration[21] and plotted in Fig. 27b consists primarily of two-jet events bunched at low S and A, with a band of three-jet events long the upper $A = 0$ axis. There are few events at large aplanarity. These data have been used by the TASSO group to search for evidence of heavy spin–1/2 quarks, but have not been analyzed yet to place limits on scalar quark production. To see what limits might be obtained, we can make a simple (and perhaps dangerous) extension of the published results. In the TASSO analysis, the fraction of events with aplanarity greater than a certain value ($A > 0.18$ is used in this case) is found from the data and is compared to the fraction that would be expected if, in addition to the five known quarks, a new heavy charged 1/3 quark were being produced with the standard point cross section,

$$R(e^+e^- \to Q^+Q^-) = e_Q^2 \, \beta(3 - \beta^2)/2 \quad . \tag{24}$$

This comparison is summarized in Fig. 28. The presence of a new spin–1/2 quark would increase the fraction of events with large aplanarity to the value shown in the figure. The data clearly rule out such a new particle with mass up to nearly the beam energy 17 GeV. We can estimate the effect that a scalar quark would have on this fraction if we assume that its decay is similar to that of a normal quark. This leads to the curve shown in the figure for the charged 2/3 case, and would rule out the region $m_{\tilde{q}} \lesssim 13 GeV$. This certainly needs to be analyzed more thoroughly to include the proper production and decay distributions for scalar quarks, and also to examine the uncertainties in the QCD prediction, which might be substantial. It seems, though, that it may be possible to set interesting limits.

The best existing constraints on scalar quark masses are inferred from hadron spectroscopy and studies of heavy quark decays. Light scalar quarks would produce an entire spectrum of $qq\tilde{q}$ baryons and $q\bar{\tilde{q}}$ mesons. The absence of these

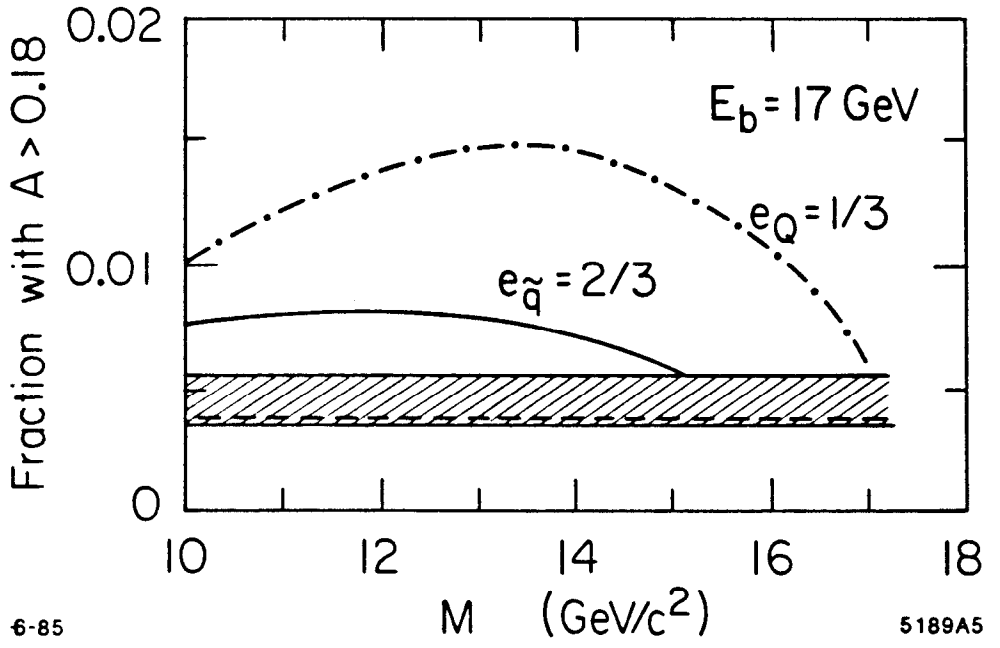

Figure 28. Fraction of hadronic events with aplanarity greater than 0.18. Shaded region is the range allowed by the data ($\pm 1\sigma$ around the mean value). Dashed line is the QCD expectation for the known five quarks and gluons. Solid curve is the estimated fraction that would be observed if, in addition to five quarks, there were also a charge 2/3 scalar quark of mass M.

states requires $m_{\tilde{q}} \gtrsim 1 - 2$ GeV. We can do slightly better by noting that the existence of a light superpartner to the charm or bottom quark would disrupt the decay distributions of these fermions. For example, if $m_{\tilde{b}} < m_b$ then the electromagnetic decay shown in Fig. 29 would dominate the b-quark lifetime. The lepton spectrum, shown in Fig. 30, fairly well establishes, however, that the b-quark decays primarily through the Cabibbo-suppressed weak charged current to a charm quark.[22] Furthermore, the b-quark lifetime is longer than would be expected if it had an electromagnetic decay.[23]

The conclusion that should be drawn from this discussion is that scalar quark masses are not very well constrained. Studies of shape parameters in e^+e^- hadronic events, or perhaps of momentum distributions of leptons found in these events, may be able to rule out the existence of scalar quarks with $m_{\tilde{q}} \lesssim$ 15 GeV, but no limits have been reported in the literature.

D. Gluinos

The spin-1/2 superpartner of the gluon can be produced as a secondary particle in two and three-jet processes as shown in Fig. 31a and Fig. 32a. Neither of these will lead to an easily discernable signal. The bremsstrahlung process in Fig. 31a, and subsequent decay of the gluino into $q\bar{q}\tilde{\gamma}$ (Fig. 31b), will yield two photinos in the final state, but the multiplicity of quarks is large, so the missing energy is small. The process shown in Fig. 32 results in a three-jet event which might be analyzed[24] to extract the Ellis-Karliner angle $\tilde{\theta}$ defined in Fig. 32b. If it were possible to isolate the gluino by a combination of topological and missing energy requirements, then the distribution of $\tilde{\theta}$ would be that shown in Fig. 33 for the spin-1/2 to spin-1/2 + scalar decay. This appears to be extremely difficult.

A more interesting possibility is to look for bound states of $\tilde{g}\tilde{g}$ produced in radiative decays of heavy quarkonium.[25,26] Two possible ways to produce a gluinonium bound state (glueballino ?) are shown in Fig. 34. The gluino is a self-conjugate fermion so the $\tilde{g}\tilde{g}$ state is antisymmetric and must have even charge conjugation parity. Furthermore, the $\tilde{g}$ is a color octet state, so the ground state

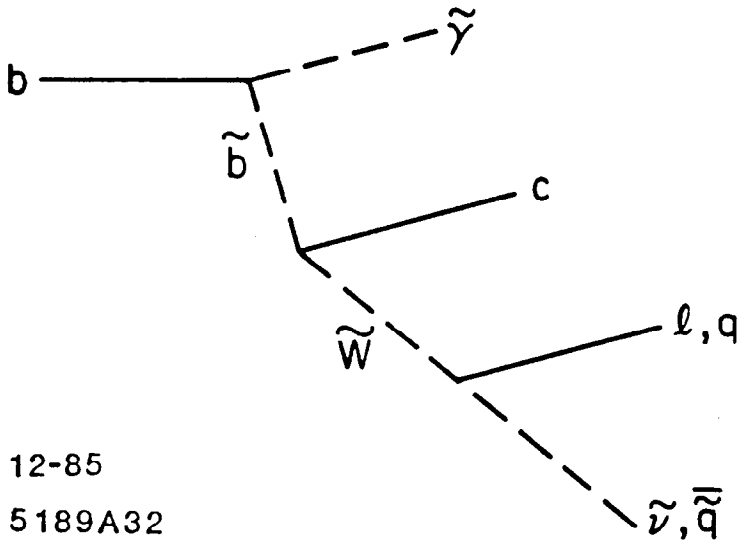

Figure 29. Decay of a b-quark that would dominate the b lifetime if $m_{\tilde{b}} < m_b$.

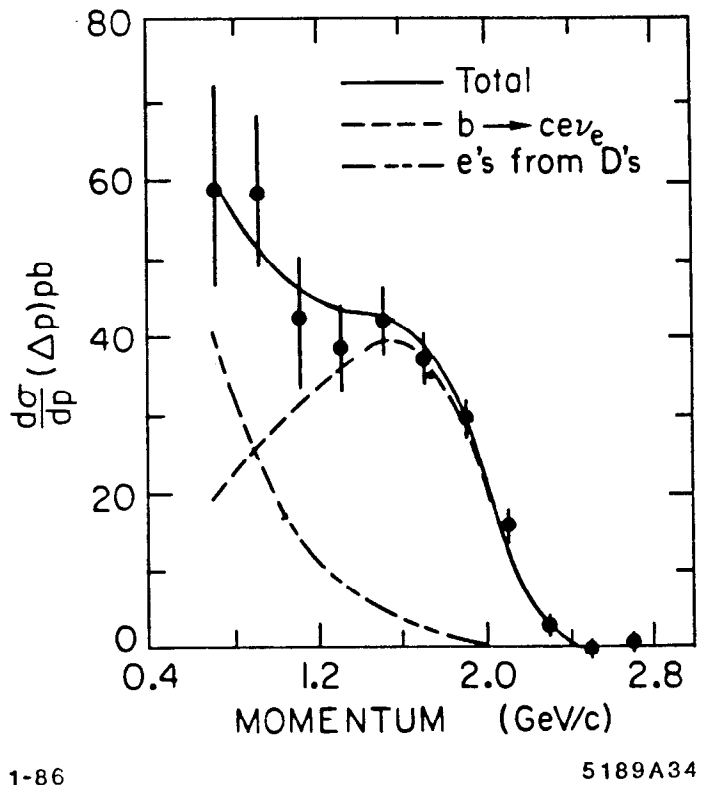

Figure 30. Spectrum of electrons from *b*-quark decays.

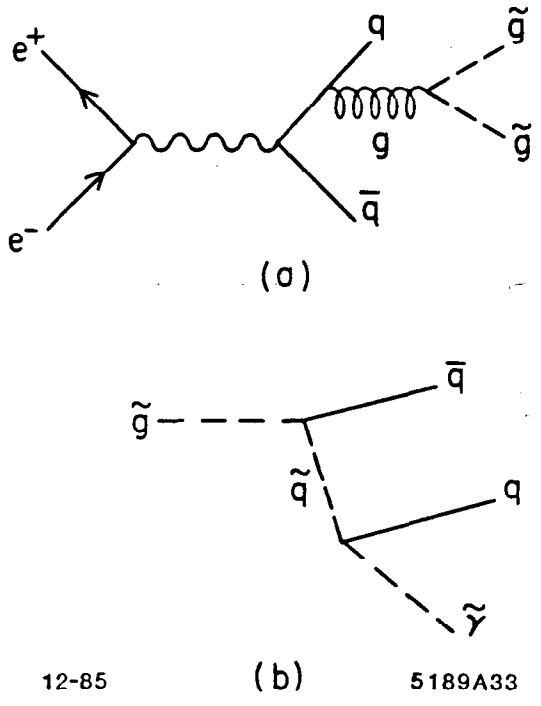

Figure 31. (a) Bremsstrahlung production of gluino pairs. (b) Gluino decay.

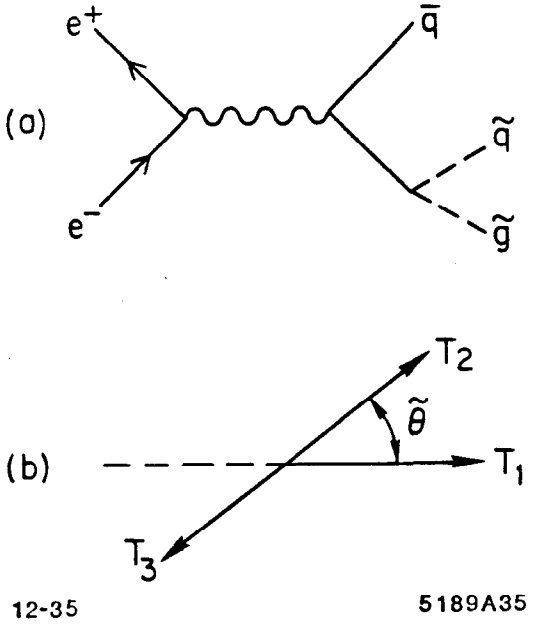

Figure 32. (a) The process $e^+e^- \to \bar{q}\tilde{q}\tilde{g}$. (b) Ellis-Karliner angle. T_1 is the principle thrust axis. The reference frame is boosted along T_1 to align T_2 and T_3.

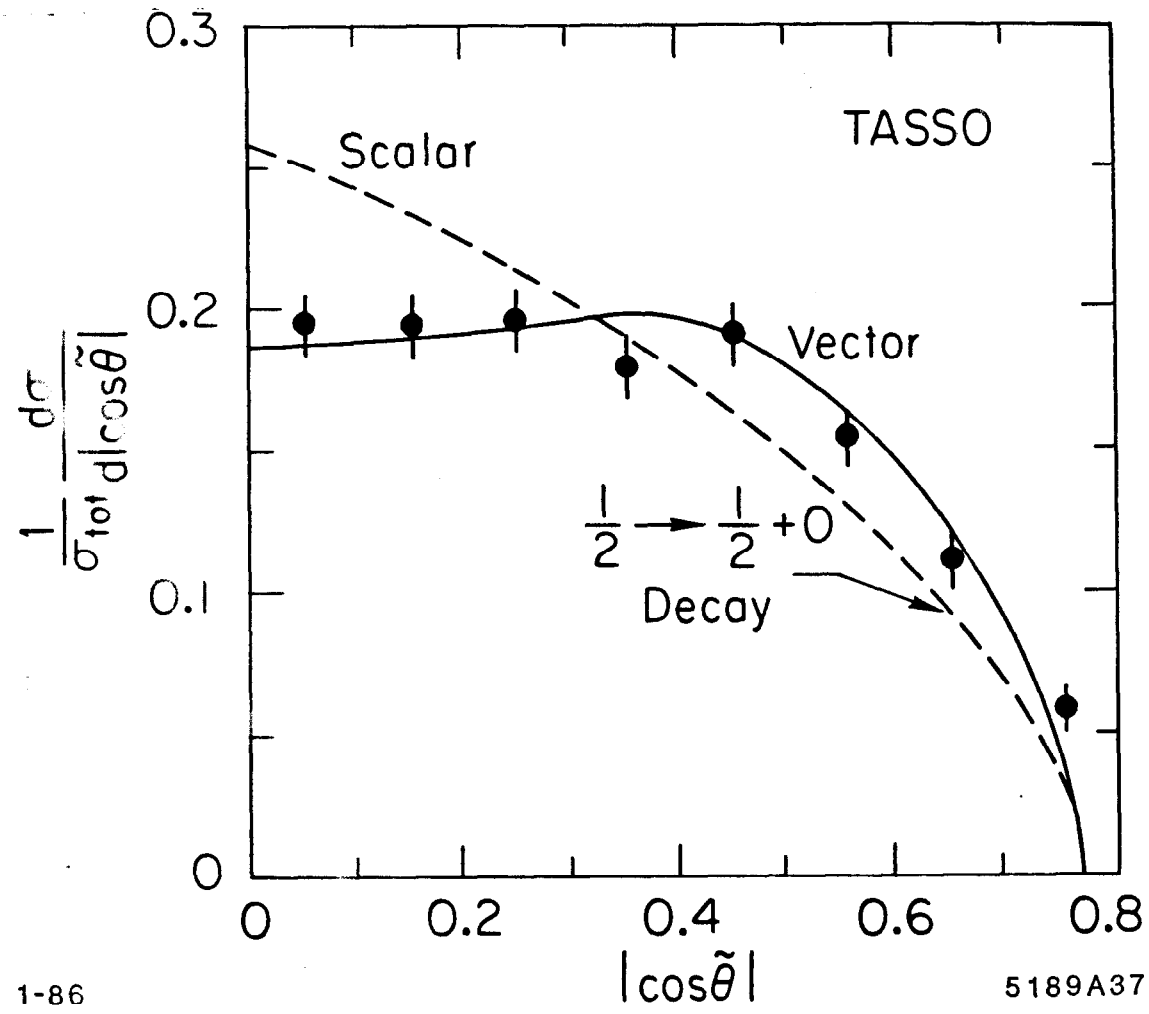

Figure 33. Distribution of the Ellis-Karliner angle observed in three-jet events compared with that expected if the spin of the gluon is 1. The $e^+e^- \rightarrow \tilde{q}\tilde{q}\tilde{g}$ process would follow the $\frac{1}{2} \rightarrow \frac{1}{2} + 0$ curve.

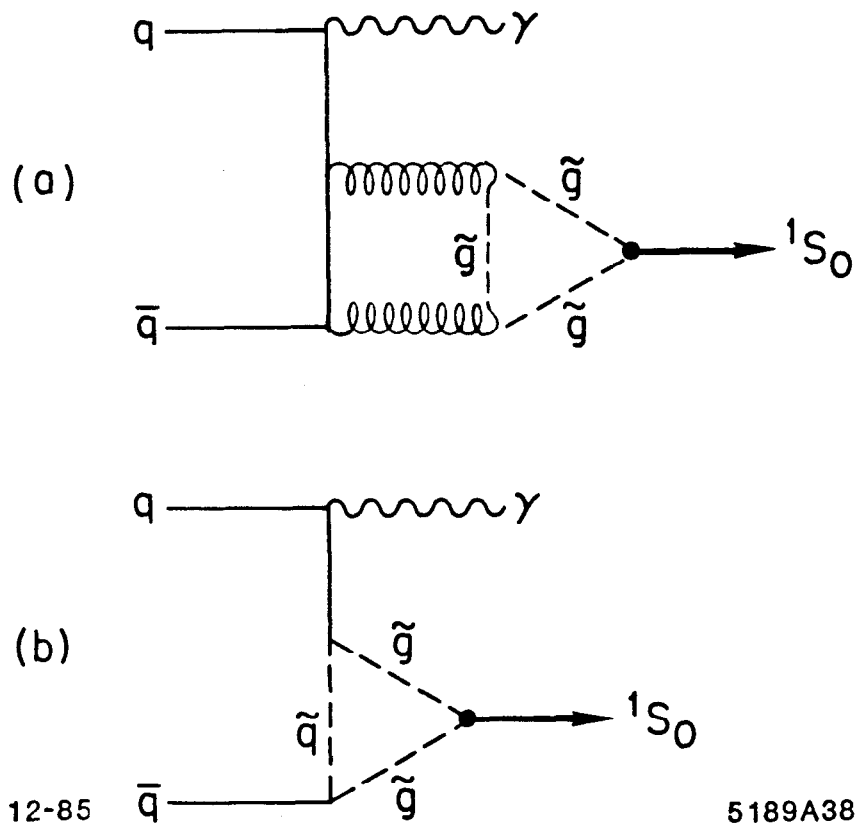

Figure 34. Gluinonium bound state production in decays of $^3S_1$ quarkonium.

of the color singlet combination will be generated through an S-wave interaction. It's important to notice that, unlike the gluon, there is no triple gluino vertex. The decay of a $\tilde{g}\tilde{g}$ state must proceed by the exchange diagram shown in Fig. 35, and will have a Zweig-like suppression if the mass of the gluino is not small.

With these properties, the gluinonium ground state, denote it $\tilde{\eta}_g$, will be similar to the charmonium 0^{-+} state $\eta_c(2980)$, except that it is made of colored constituents. The binding potential will be strengthened by color factors

$$V_{\tilde{g}\tilde{g}} \approx 9/4\, V_{q\bar{q}} \quad , \tag{25}$$

which will enhance the amplitude of the wavefunction at the origin relative to that of a similar quarkonium state,

$$|R_{\tilde{\eta}_g}(0)|^2 \approx 3 - 4\,|R_{\eta_q}(0)|^2 \quad . \tag{26}$$

Estimates of the total width, made using the formula,

$$\Gamma(\tilde{\eta}_g \to gg) = \frac{18\alpha_s^2}{m^2_{\tilde{\eta}_g}} |R_{\tilde{\eta}_g}(0)|^2 \quad , \tag{27}$$

yield[26]

$$\Gamma_{\tilde{\eta}_g} \sim 50 - 300 \text{ MeV} \tag{28}$$

for $m_{\tilde{\eta}_g}$ ranging downward from 10 GeV/c^2 to 2 GeV/c^2.

The branching ratio of the $^3S_1$ quarkonium ground state into $\gamma\tilde{\eta}_g$ has been estimated as,[26]

$$BR(^3S_1 \to \gamma\tilde{\eta}_g) = \frac{\alpha_s \alpha e_Q^2}{m_{\tilde{\eta}_g} m_V^2} \cdot |R_{\tilde{\eta}_g}(0)|^2 \cdot f(m_V, m_{\tilde{\eta}_g}) \tag{29}$$

where e_Q is the charge of the initial quark type and m_V is the mass of the quarkonium state. The function f depends only mildly on the values of m_V and

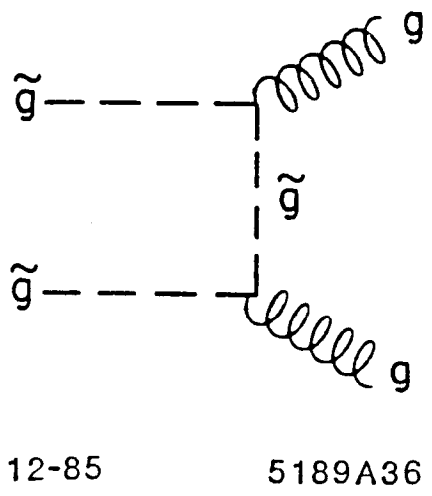

Figure 35. Decay of a gluinonium bound state.

$m_{\tilde{\eta}_g}$. This can be normalized to the decay into the 0^{-+} pseudoscalar quarkonium state

$$\frac{\Gamma(^3S_1 \to \gamma\tilde{\eta}_g)}{\Gamma(^3S_1 \to \gamma\eta_q)} = \frac{27}{4} \cdot \frac{|R\tilde{\eta}_g(0)|^2}{|R\eta_q(0)|^2} \cdot f'(m_{\tilde{\eta}_g}, m_{\eta_q}) \quad . \tag{30}$$

The 27/4 is a color factor. From Eq. (26) and with f' taken from Ref. 26,

$$\Gamma(^3S_1 \to \gamma\tilde{\eta}_g) \approx 20 \cdot \Gamma(^3S_1 \to \gamma\eta_q) \tag{31}$$

for gluinos with $m_{\eta_{\tilde{g}}} \approx m_{\eta_q}$. As an example, the branching ratio for J/ψ into $\gamma\eta(550)$ is 0.1%, so we would expect $\mathrm{BR}(J/\psi \to \gamma\tilde{\eta}_g) \approx 1\%$, which is quite large.

The decay of the $\tilde{\eta}_g$ is primarily to two gluons (Fig. 35). Light quarks will appear in approximately equal numbers of decays, while heavy quarks may suffer some suppression of available phase space. If the mass of the $\tilde{\eta}_g$ is less than ~ 2 GeV/c^2, then it will mix with other 0^{-+} states. This has been one of the difficulties in the identification of gluonium candidates and would be no less of one in the case of the $\tilde{\eta}_g$. At larger masses the situation is not as complicated. The width of the $\tilde{\eta}_g$ is expected to be more narrow (Eq. 28) and there are fewer 0^{-+} $q\bar{q}$ states. The CUSB Collaboration has looked for monochromatic photons in decays of the $\Upsilon(9460)$. No signal corresponding to hadronic masses above 2 GeV/c^2 has been found[5,27]; the limits are given in Fig. 36 along with the expected branching ratio of the $\tilde{\eta}_g$. It can be seen that the experiment is not yet sensitive to the expected signal, but perhaps will be in the future.

E. Scalar Neutrinos

In our discussions of charged scalar leptons we have been careful to take account of the possible mixing between the superpartners of left and right-handed Dirac states. Since only left-handed neutrinos are observed in nature, we only consider the case of a single scalar neutrino state $\tilde{\nu}_L \equiv \tilde{\nu}$.

Scalar neutrinos can be produced in pairs by e^+e^- annihilation through the standard weak neutral current (Fig. 37a) or, in the case of $\tilde{\nu}_e$, through the t-channel exchange of the superpartner of the weak boson (Fig. 37b). The Z^0

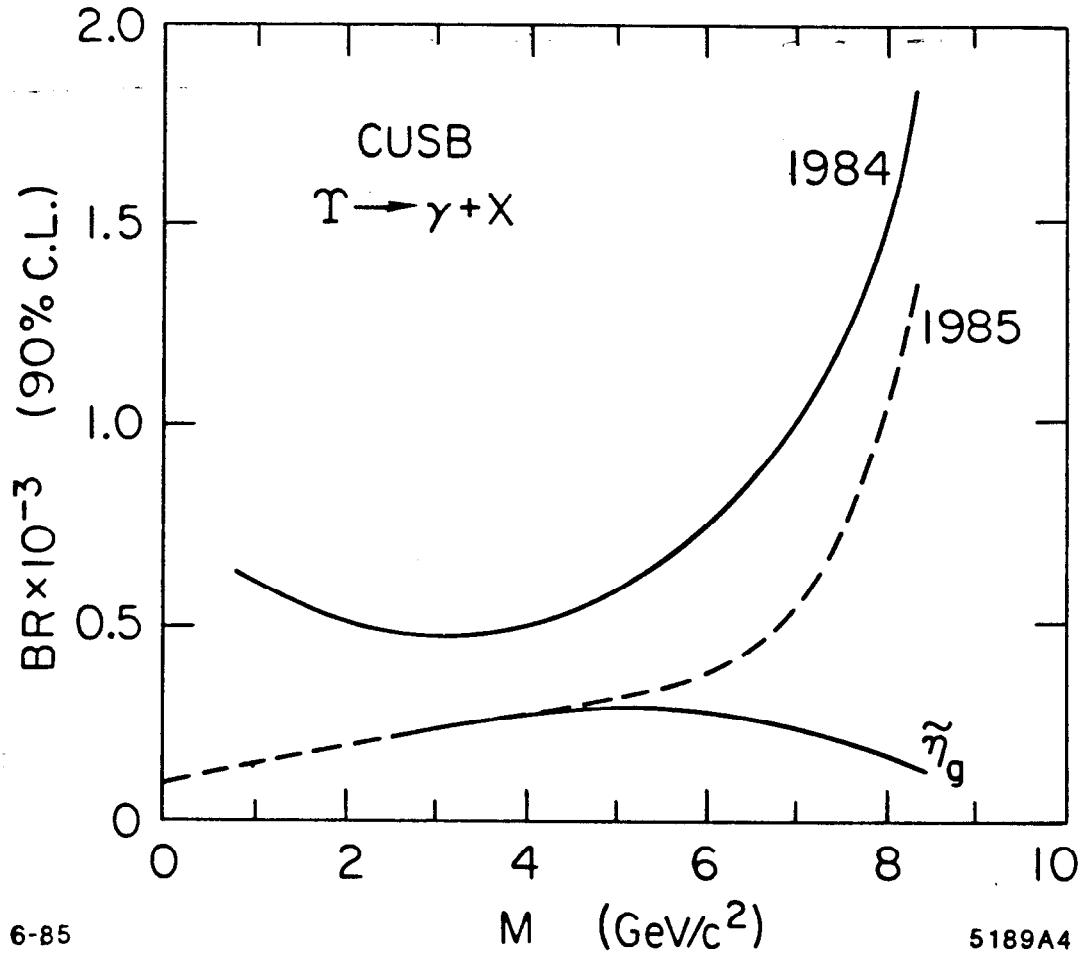

Figure 36. Limits on production of narrow states in radiative decays of the upsilon.

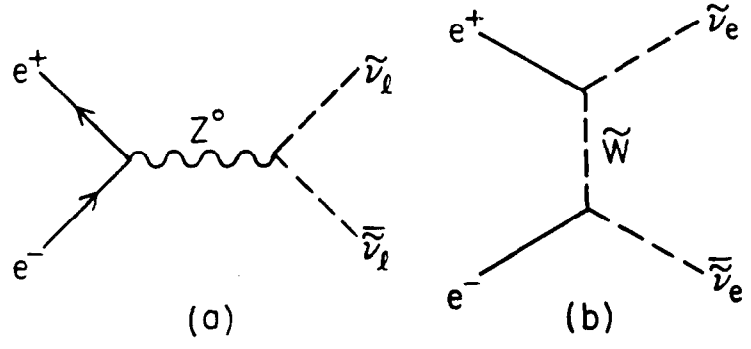

Figure 37. Pair production of scalar neutrinos in e^+e^- annihilation.

partial width created by a scalar neutrino is given by[28]

$$\Gamma(Z^0 \to \tilde{\nu}\bar{\tilde{\nu}}) = \frac{1}{2}\,\beta^3\Gamma(Z^0 \to \nu\bar{\nu}) \quad . \tag{32}$$

At PEP/PETRA this corresponds to the production of $\approx$ 20 pairs per species (with $\beta = 1$) in a data sample of 100 pb^{-1}. The t-channel diagram can be important for the production of ν_e if the mass of the $\widetilde{W}$ is not too large; for $m_{\widetilde{W}} \approx m_W$ we can expect $\approx$ 100 $\tilde{\nu}_e\bar{\tilde{\nu}}_e$ pairs in the same data sample.

Clearly if the mass of the $\tilde{\nu}$ is zero (or small), then it will be stable. In that event it can only be detected by a measurement of the cross section for the radiative process

$$e^+e^- \to \gamma\tilde{\nu}\bar{\tilde{\nu}} \quad . \tag{33}$$

We've already discussed this experimental technique, but it's worth pointing out that, if a signal in this channel is observed, it will be important to determine not only the size of the cross section, but also it's dependence on beam energy. Photinos are produced through the electromagnetic interaction with a different dependence on $\sqrt{s}$ than that expected for scalar neutrinos.

Possible decay modes of a massive $\tilde{\nu}$ are shown in Figures 38 and 39 . These can become rather intricate. If the mass of the $\tilde{\nu}$ is larger than the mass of the photino, then the decays in Fig. 38 result in all neutral, and invisible, final states. The lifetime for these decays is given by[29]

$$\tau_{\tilde{\nu}} \approx \frac{10^{-16}}{m_{\tilde{\nu}}}\,\frac{1}{F^2}\ \text{sec} \tag{34}$$

where the structure function F depends upon masses of the scalar leptons. For $m_{\tilde{l}} \approx m_W$ and $m_{\tilde{\nu}} << m_W$ it turns out that F^2 is of order unity, and $m_{\tilde{\nu}}$ must be $\lesssim$ 1 MeV to generate $\tau_{\tilde{\nu}} \gtrsim 10^{-13}$ sec.

—If the mass of the $\tilde{\nu}$ is large enough, then the charged decay channels shown in Fig. 39 become open. The lifetime will become $< 10^{-13}$ sec. If the gluino is

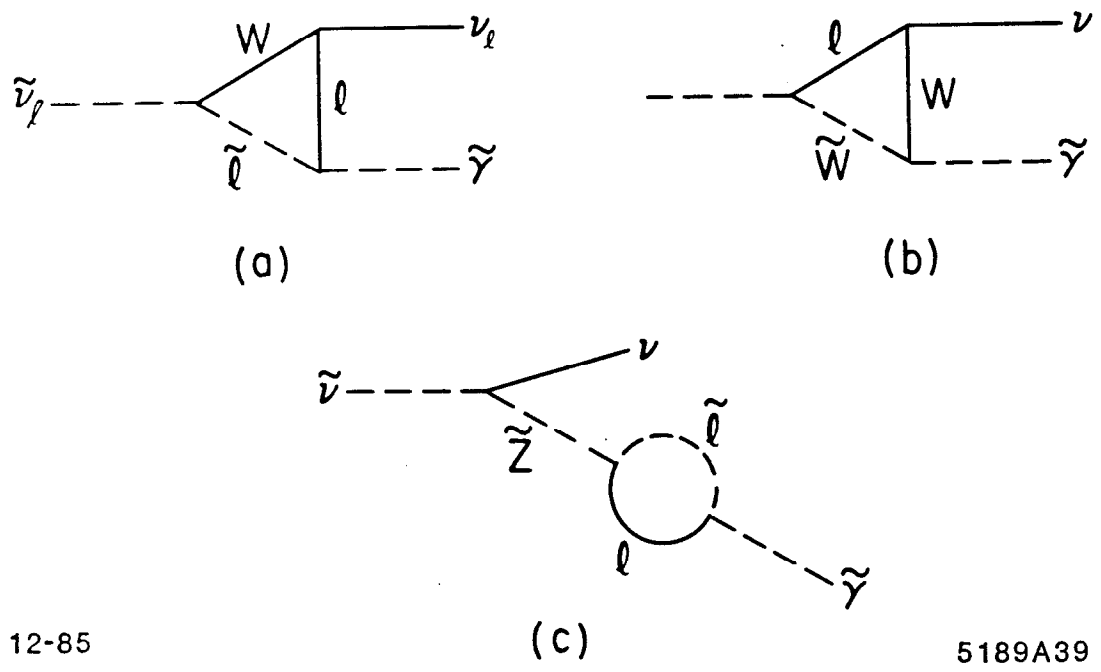

Figure 38. All neutral decays of scalar neutrinos.

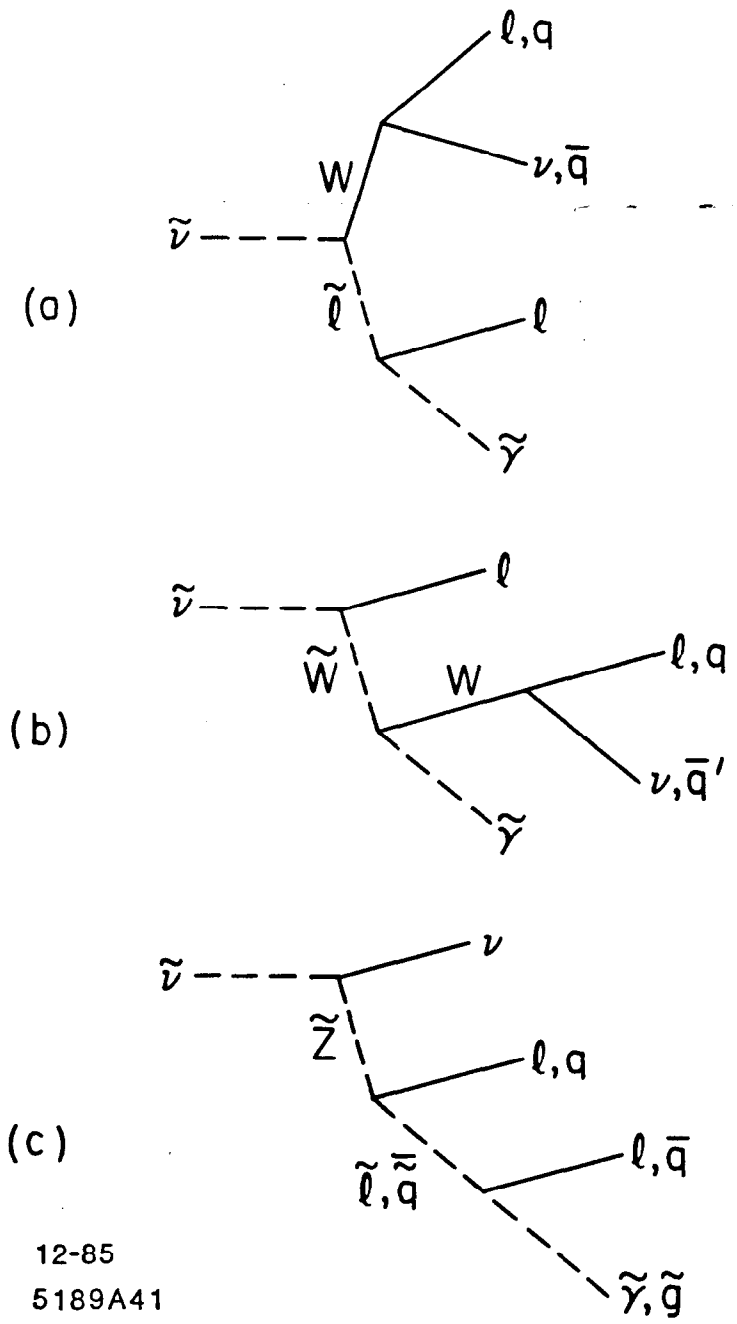

Figure 39. Charged decays of scalar neutrinos.

light and $m_{\tilde{q}} \approx m_{\tilde{\ell}}$, then (c) will dominate (unless $m_{\tilde{g}} >> m_W$). One estimate, for example, gives[29]

$$\begin{aligned} &BR(\tilde{\nu} \rightarrow \text{hadrons}) \sim 80\% \\ &BR(\tilde{\nu} \rightarrow \text{leptons only}) \sim 1\% \\ &\text{remainder are } \nu\tilde{\gamma} \quad . \end{aligned} \tag{35}$$

If the gluino is heavy, then diagram (a) may become dominant and the $\tilde{\nu}$ decay look similar to that of a heavy neutrino.

The hadronic decays generate essentially no signature by themselves because the missing energy is not large. The scalar neutrinos are produced in pairs, however, so a very clear signature can be left if one of the $\tilde{\nu}$ decays to $\nu\tilde{\gamma}$, and the other decays to charged particles. This topology appears in a detector as a single isolated monojet with a large missing momentum. There have been searches for monojet events at PEP and PETRA, but they are not completely independent of assumptions about the decay characteristics of the parent particles. They depend most sensitively upon the particle masses involved. Shown in Fig. 40a is an example of a set of limits obtained from results reported by the Mark II Collaboration.[30] (The published numbers have been rescaled to produce the curve displayed in the figure.) What is plotted is the limit on the fraction of $\tilde{\nu}\bar{\tilde{\nu}}$ events that contain one all-neutral decay and one all-charged decay that is consistent with the limit placed by the experiment on monojet production. A sample calculation[29] of the expected fraction is shown in Fig. 40b for the choices $\tilde{\nu}_e = 5$ GeV/c^2 and $m_{\widetilde{W}} \approx m_W$. At small values $m_{\tilde{q}} << m_{\tilde{\nu}_e}$, the $\tilde{\nu}$ decays mostly into hadronic final states, while at large mass $m_{\tilde{q}} >> m_{\tilde{\nu}_e}$ the $\tilde{\nu}$ decays are primarily into $\nu\tilde{\gamma}$. It would appear that some range of $m_{\tilde{q}}$ and $m_{\tilde{\nu}_e}$ could be ruled out, but notice that the expected production and decay rates depend also upon the unknown masses of other supersymmetric particles (i.e. $m_{\widetilde{W}}$, $m_{\tilde{\gamma}}$, and $m_{\tilde{g}}$).

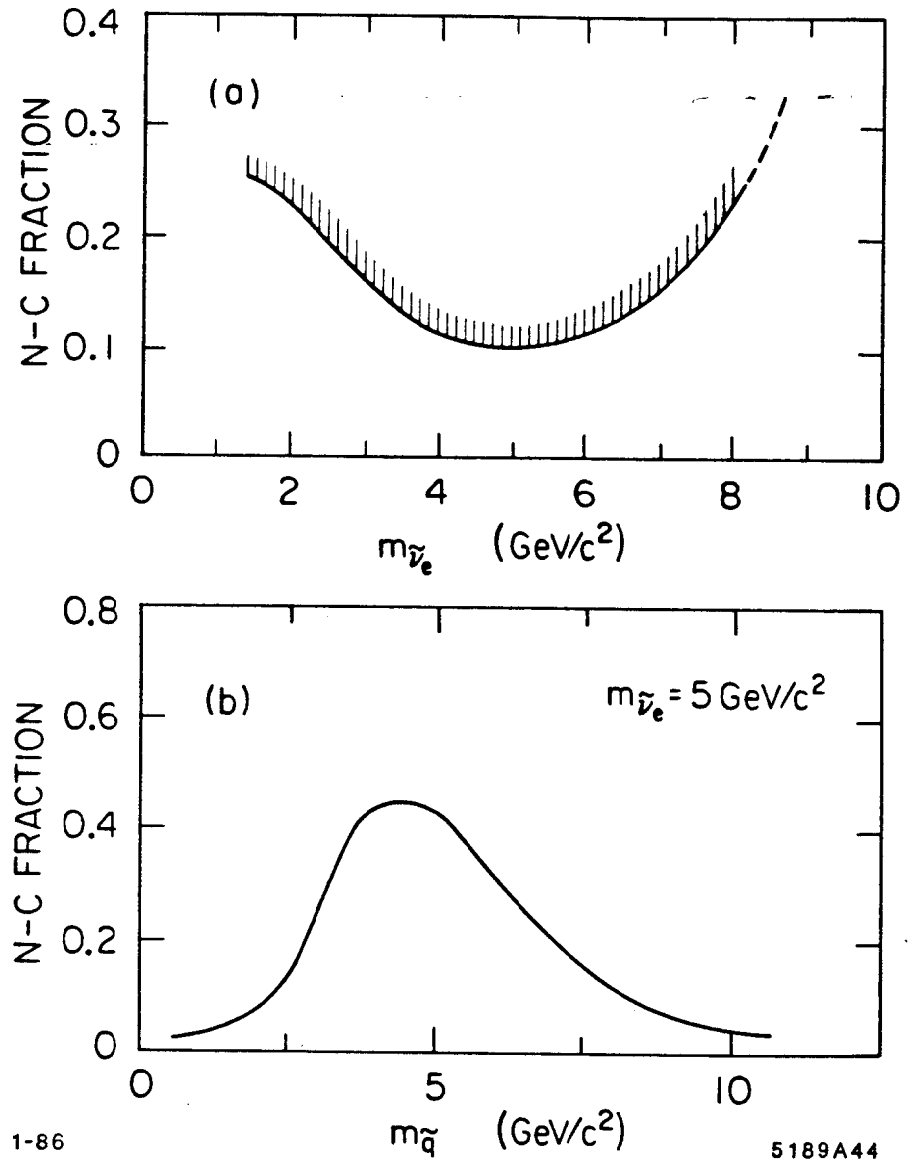

Figure 40. (a) Limits on one-sided charged decays of $\tilde{\nu}\bar{\tilde{\nu}}$ pairs. (b) Expected one-sided charged decays of scalar electron neutrino pairs.

A less convoluted, if not more limited, analysis can be done of $\tau^{\pm}$ decays to search for evidence of a scalar $\tilde{\nu}_\tau$. If $m_{\tilde{\nu}_\tau} < m_\tau$ and if there exists another $\tilde{\nu}_\ell$ with $m_{\tilde{\nu}_\ell} < m_\tau$, then the decay shown in Fig. 41a will proceed with a partial width[31]

$$\frac{d\widetilde{\Gamma}}{dx} = \frac{G_F^2 m_\tau^5}{4\pi^3}\left(\frac{m_W}{m_{\widetilde{W}}}\right)^4 \widetilde{F}(x) \qquad (36)$$

where x is the lepton momentum fraction and $\widetilde{F}(x)$ is the momentum distribution for a three-body decay. There are constraints imposed on the size of this potential decay channel by measurements of the τ lifetime, the final state lepton spectrum in τ decays, and the leptonic branching ratio of the τ; the τ behaves in every way like a sequential lepton in the Standard Model. One analysis of the experimental data[31] yields the limits shown in Fig. 42. These can be approximately summarized by the requirement

$$m_{\tilde{\nu}_\tau} + m_{\tilde{\nu}_\ell} > m_\tau \qquad (37)$$

if $m_{\widetilde{W}} \lesssim m_W$.

F. Gauginos and Higgsinos

Because of the complexity introduced by possible mixing of weak interaction eigenstates, searches for evidence of the gauge sector of supersymmetry become more generic than the searches that we've discussed so far. The weak isospin structure of these particles is displayed in Table IV. All of the $R = -1$ superpartners are spin–1/2 fermions, and all exhibit normal electroweak couplings. For example, the Higgsino coupling is proportioned to the mass of the fermion at the vertex,

$$g(f\bar{\tilde{f}}\widetilde{H}) \sim m_f \quad . \qquad (38)$$

The only conserved quantum number that is not common to all particles listed in Table IV is the electric charge. States with common charge will mix to form

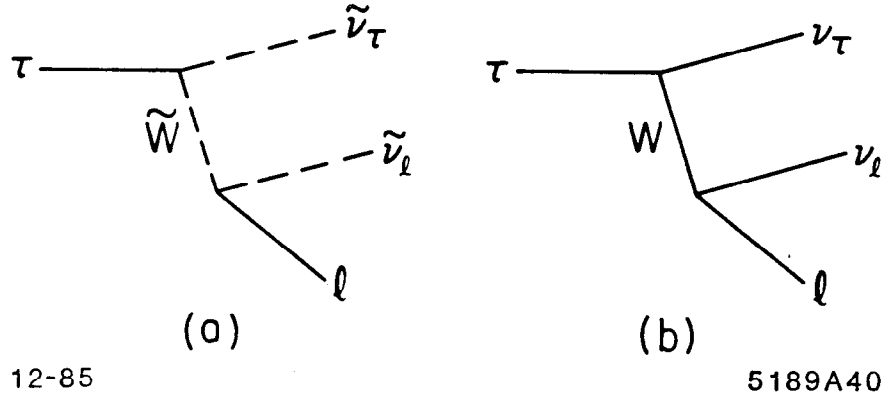

Figure 41. Tau decays into scalar tau neutrinos compared with normal tau decay.

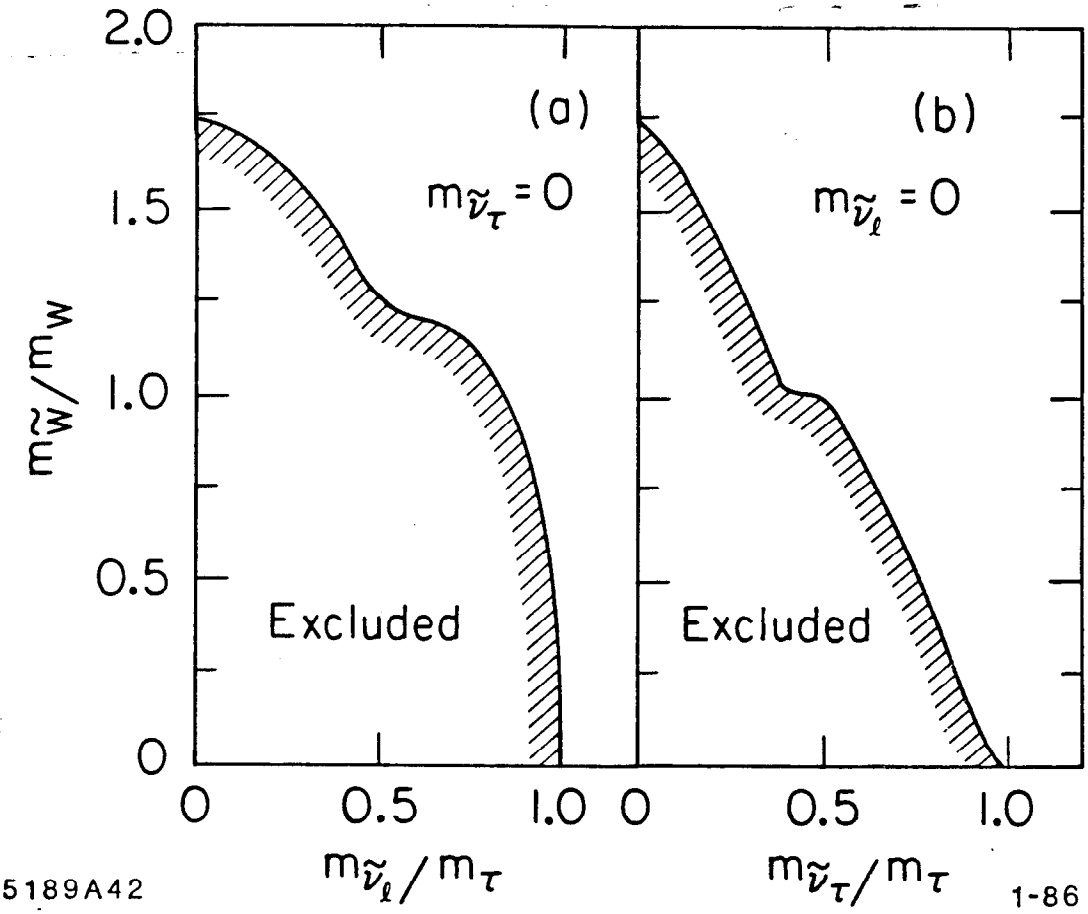

Figure 42. Limits on scalar neutrino masses inferred from properties of tau decays.

TABLE IV

Weak isospin structure of gauginos and Higgsinos

Triplet: $(T_3 = \pm 1,\ 0)$	$(W^{\pm},\ W_3^0) \longleftrightarrow (\widetilde{W}^{\pm},\ \widetilde{W}_3^0)$
Doublets: $(T_3 = \pm 1/2)$	$\begin{pmatrix} H_1^+ \\ H_1^0 \end{pmatrix} \begin{pmatrix} H_2^0 \\ H_2^- \end{pmatrix} \longleftrightarrow \begin{pmatrix} \widetilde{H}_1^+ \\ \widetilde{H}_1^0 \end{pmatrix} \begin{pmatrix} \widetilde{H}_2^0 \\ \widetilde{H}_2^- \end{pmatrix}$
Singlet: $(T_3 = 0)$	$B^0 \longleftrightarrow \widetilde{B}^0$

mass eigenstates. This, unfortunately, makes it possible to essentially "turn off" any particular production or decay channel that might serve as a signature for the existence of these particles.

1. Charginos

The charged gauge fermion mass eigenstates are Dirac spinors of the form

$$\tilde{\chi}_1^+ = \begin{pmatrix} C_{11} & \widetilde{W}_L^+ & + & C_{12}\tilde{H}_{2L}^+ \\ C_{21} & \widetilde{W}_R^{-*} & + & C_{22}\tilde{H}_{1R}^{-*} \end{pmatrix} \tag{39}$$

and the orthogonal state $\tilde{\chi}_2^+$. The decay $\tilde{\chi}^\pm \to \tilde{\ell}\nu$, for example, is generated by the Lagrangian

$$\mathcal{L}_{int} = -g\bar{\tilde{\chi}}\left(\frac{1-\gamma_5}{2}\right)\nu\tilde{\ell}_L^* \tag{40}$$

which projects out the $\widetilde{W}$ component of the $\tilde{\chi}$ since the mass of the neutrino is zero. Purely electromagnetic couplings must be strictly to the mass eigenstate, while the Z^0 will couple as usual to $T_3 - Q\sin^2\theta_W$.

The chargino states are fermions and can be produced in pairs in e^+e^- annihilation through the diagrams shown in Fig. 43. The photon propagator in Fig. 43a produces a cross section of one unit of R independently of mixing, and notice that i is not necessarily equal to j. The production of the $\widetilde{H}$ component of $\tilde{\chi}$ by the t-channel diagram in Fig. 43b is suppressed by the electron mass.

Possible decay channels of charginos are assembled in Fig. 44. The strong decay is expected to be dominant unless suppressed by kinematics, while the two-body weak decays (b and d) could be as much as 20%. The three-body leptonic piece (c) is likely to be small. It is not likely that the hadronic decays of these particles have been missed at PEP and PETRA, but if the mass of the gluino is large enough to suppress (a), and the mass of the lightest neutralino $\tilde{\chi}_1^0$ is $\gtrsim E_b/2$, then the weak decay (c) would either not be kinematically allowed, or would yield too little visible energy for the events to survive the cuts that are

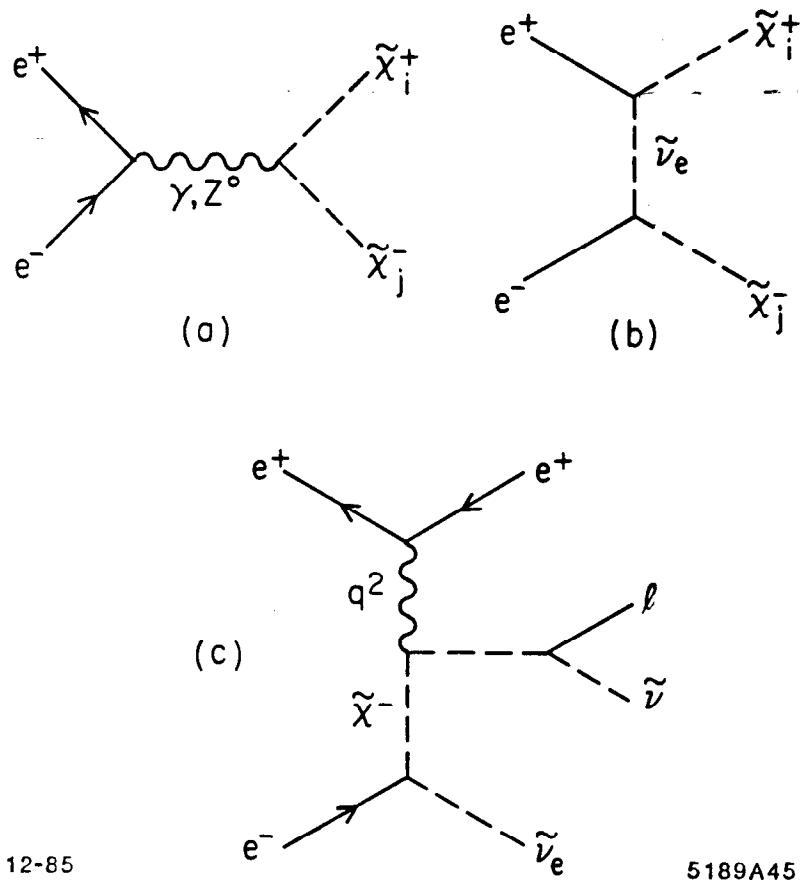

Figure 43. (a),(b) Pair production of charginos. (c) Production of a single chargino state in e^+e^- annihilation.

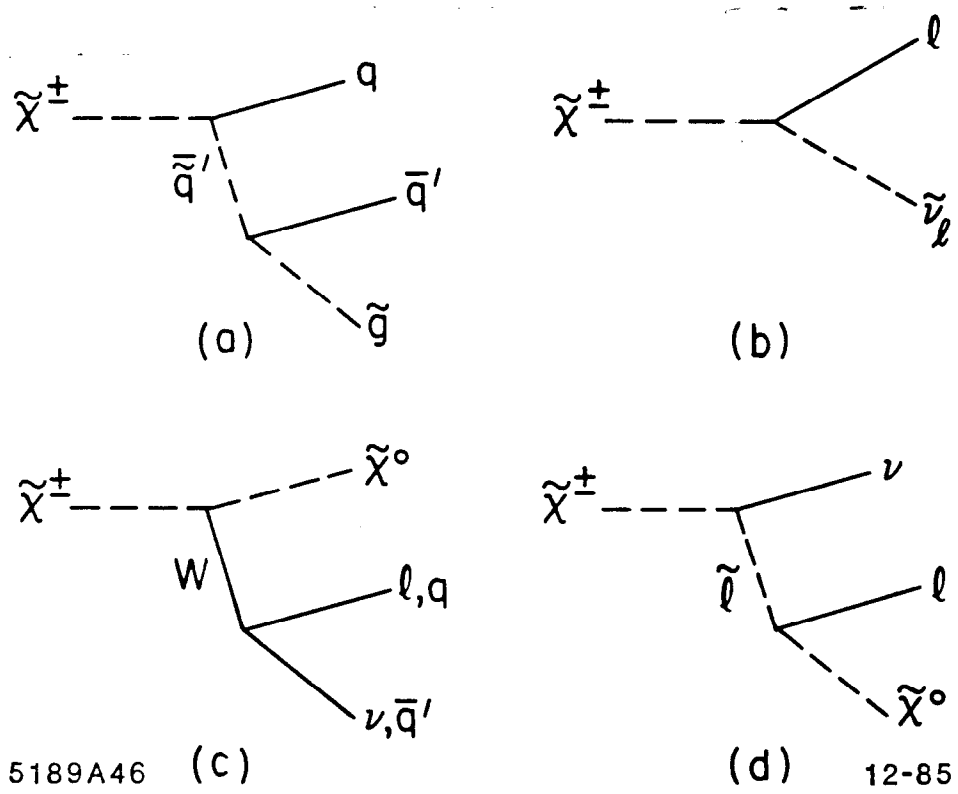

Figure 44. Decays of chargino states.

typically used to analyze hadronic final states. For example, the visible energy spectrum of events used by the MAC Collaboration[32] to measure R is shown in Fig. 45. A cut has been made at approximately 1/3 of the total center of mass energy. It would require some work to determine the limit contour in a plot of $m_{\tilde{\chi}^0}$ and $m_{\tilde{\chi}^\pm}$, but a proper analysis of the total hadronic cross section data should yield

$$m_{\tilde{\chi}^\pm} \gtrsim 20 \text{ GeV} \quad \text{for} \quad m_{\tilde{\chi}^0} \lesssim 10 \text{ GeV} \quad . \tag{41}$$

Production of $\tilde{\chi}^\pm$ pairs followed by their leptonic decay

$$\tilde{\chi}^\pm \rightarrow \ell\nu\tilde{\chi}^0 \text{ or } \ell\tilde{\nu} \tag{42}$$

would create a clear signature in the searches for scalar leptons described in Section IIIA. Production of a single chargino state by the diagram in Fig. 43c is similarly excluded by the search for single scalar electron production presented in the same discussion above. For example, the limits given by the Mark J group,[33] displayed in Fig. 46, are similar to those shown in Fig. 6a for the selectron. These limits have been obtained by simply assuming a particular leptonic decay branching fraction (10% was used), but since they are limited primarily by the beam energy and not statistics, they are not very sensitive to the assumed value. Any leptonic branching fraction larger than 2 – 3% would have generated a signal in these data.

2. Neutralinos

All four of the neutral weak eigenstates can mix with each other

$$\begin{pmatrix} \tilde{\chi}_1^0 \\ \tilde{\chi}_2^0 \\ \tilde{\chi}_3^0 \\ \tilde{\chi}_4^0 \end{pmatrix} = c_{ij} \begin{pmatrix} \tilde{B}^0 \\ \tilde{W}_3^0 \\ \tilde{H}_1^0 \\ \tilde{H}_2^0 \end{pmatrix} \tag{43}$$

to produce mass eigenstate $\tilde{\chi}_i^0$. The nature of the mixing is quite model dependent, but there is always a lightest neutral state. Take it to be $\tilde{\chi}_1^0$. This is an

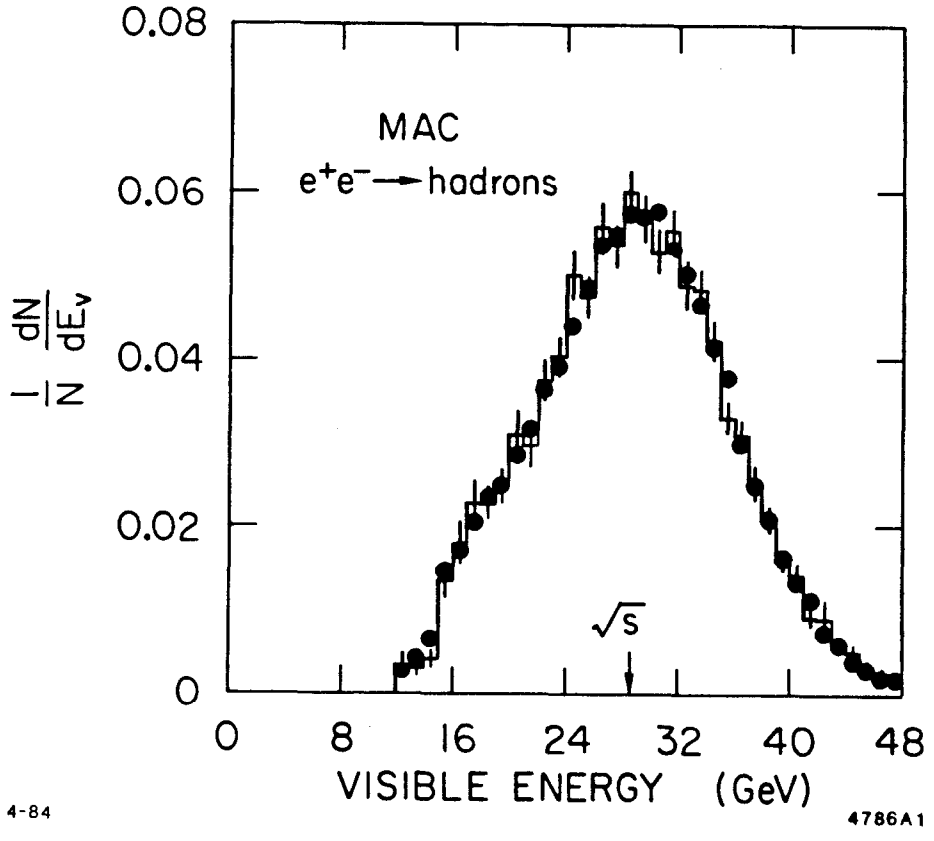

Figure 45. Visible energy from hadronic final states in the MAC detector.

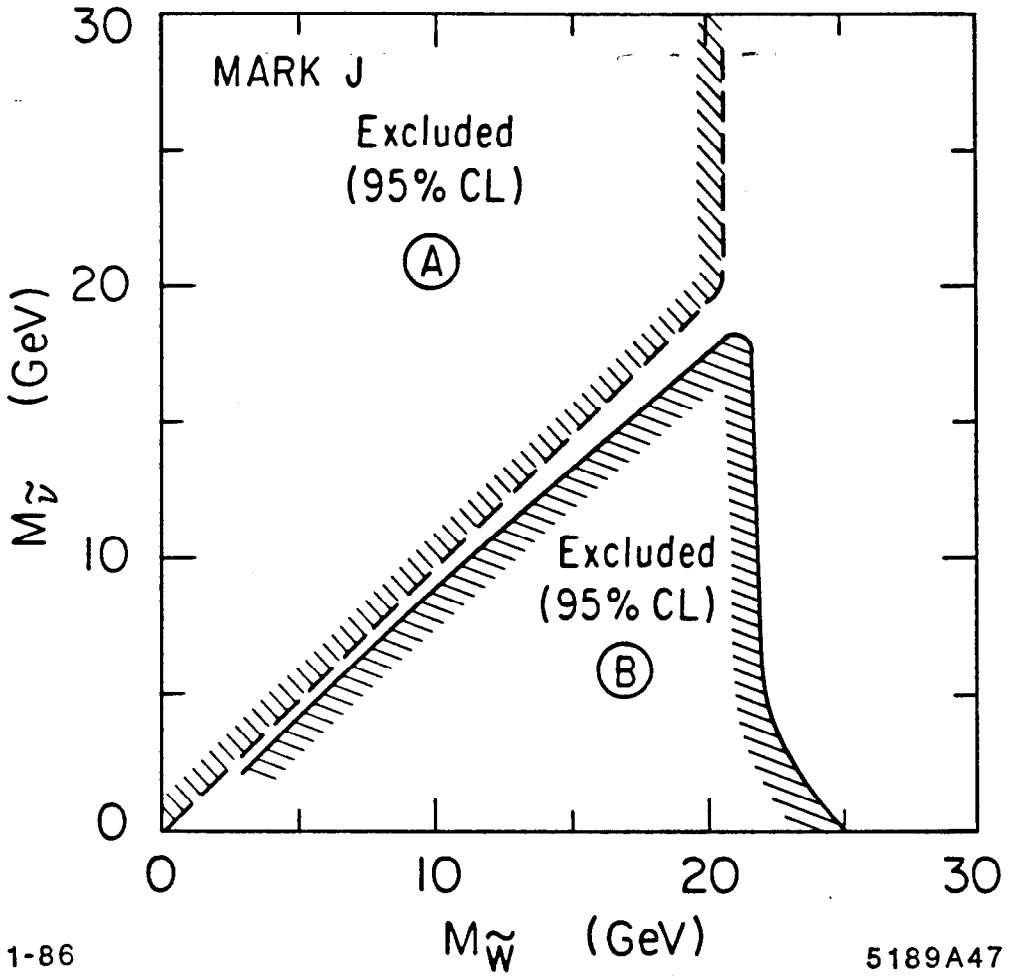

Figure 46. Limits on $\tilde{W}$ and scalar neutrino masses. Region (A): searches for stable massive charged particles. Region (B): searches for acoplanar lepton pairs or single isolated leptons.

important particle since, as we have seen, it will be stable and is one of the end products of many decay chains. It is possible that $\tilde{\chi}_1^0$ is the photino, but not necessarily so. In some models, for example, the lightest state is a Higgsino,

$$\tilde{\chi}_1^0 = \tilde{h}^0 = (v_2\tilde{H}_1^0 + v_1\tilde{H}_2^0)\Big/\sqrt{v_1^2 + v_2^2} \tag{44}$$

(v_1 and v_2 are vacuum expectation values), while in other models it contains gaugino and Higgsino components.

Neutralinos can be produced in pairs in e^+e^- annihilation through either the weak neutral current or through the t-channel exchange of a selectron. The Higgsino component is not produced efficiently by the latter process, while the Z^0 couples to $T_3 - Q\sin^2\theta_W$ which is zero for both of the gauge components $\widetilde{W}_3^0$ and $\widetilde{B}^0$.

Possible decay modes of all but the lightest neutralino are shown in Fig. 47. We will denote by $\tilde{\chi}_2^0$ any neutralino except the lightest. The first graph will be small if $\tilde{\chi}_2^0$ is predominantly Higgsino unless the fermion mass m_f is large. The second graph will similarly generate decays through the gaugino component of the neutralino, while as noted above, the Z^0 will couple solely to the Higgsino component of $\tilde{\chi}_2^0$. What should be recognized from this discussion is that these decays are terribly convoluted with unknown masses and mixing parameters, so experimental results should be presented in terms of simple branching ratios, or at least, simple models which can easily be reinterpreted in terms of other models.

There are several distinctive event topologies that would be generated by neutralino pair production more or less independently of masses and mixing. They arise from the following combinations of $\tilde{\chi}_1^0$ and $\tilde{\chi}_2^0$

$$e^+e^- \to \tilde{\chi}_1^0\tilde{\chi}_1^0 \tag{45}$$

$$e^+e^- \to \tilde{\chi}_1^0\tilde{\chi}_2^0 \tag{46}$$

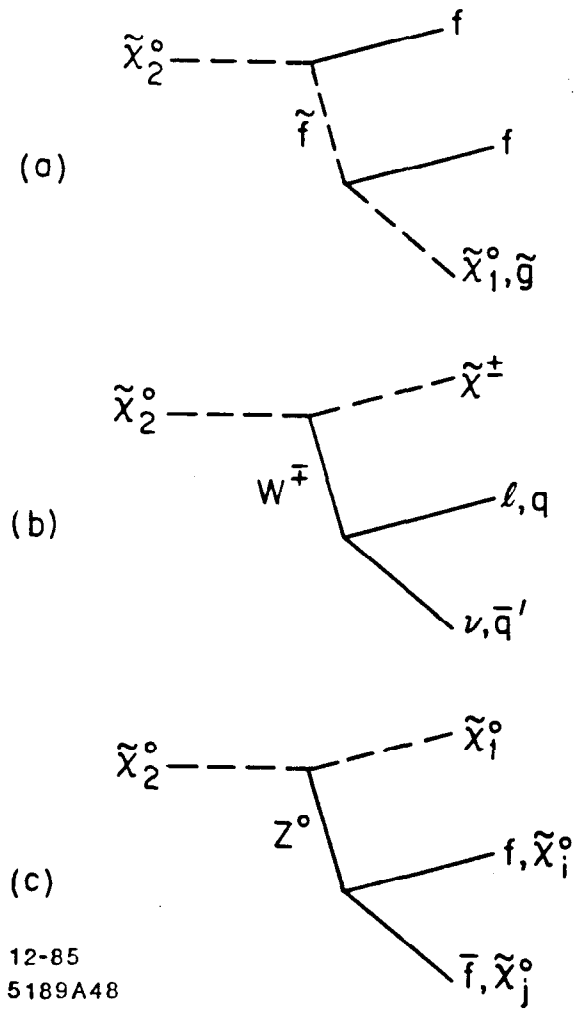

Figure 47. Neutralino decays.

$$e^+e^- \rightarrow \tilde{\chi}_2^0\tilde{\chi}_2^0 \quad . \tag{47}$$

Process (45) is just the generalization of the photino pair production channel that we have discussed in Section IIIB. Process (46) will lead to a monojet, or perhaps an energetic lepton pair, with a large momentum imbalance. Searches for these topologies have all been negative. The HRS Collaboration[34] has presented limits on the monojet final state and interpreted their results within the framework of a particular model. They assume $\tilde{\chi}_1^0$ is a massless photino and

$$\tilde{\chi}_2^0 = \lambda^2 \tilde{Z}^0 + (1-\lambda^2)\,\tilde{H}^0 \quad . \tag{48}$$

The assumption that $\tilde{\chi}_1^0$ is the photino means that only the t-channel exchange of the selectron will contribute to the production rate, so the observable cross section is

$$\sigma \cdot BR \approx 0.6(1-R^2)\left(1+\frac{R}{2}\right)\lambda^2\left(\frac{m_W}{m_{\tilde{e}}}\right)^4 \cdot BR \tag{49}$$

where $R = m_{\tilde{\chi}}^2/s$ and $\sigma \cdot BR$ will have units of picobarns. The limits, which depend upon $m_{\tilde{e}}$, $m_{\tilde{\chi}_2^0}$ and the product $\lambda^2 \cdot BR$, are given in Fig. 48. Notice that, when the mixing parameter λ^2 becomes small, $\tilde{\chi}_2^0$ becomes mostly Higgsino and the sensitivity of the experiment is reduced in this model.

Events of the type (46) in which the $\tilde{\chi}_2^0$ state decays to a lepton pair would be easily recognized in most detectors. In a manner similar to their handling of the search for charginos (Fig.46), the MARK J Collaboration[33] has assumed a 10% branching fraction for $\tilde{\chi}_2^0 \rightarrow \ell^+\ell^-\tilde{\chi}_1^0$ and arrived at the limits shown in Fig. 49. Even with the simplifying assumption for the leptonic branching fraction, the limits still must be considered as functions of three parameters, $m_{\tilde{e}}$, $m_{\tilde{\chi}_1^0}$, and $m_{\tilde{\chi}_2^0}$.

Process (47) will be difficult to discover unless the neutralino state has a large branching fraction into two leptons. Then a useful number of four-lepton event with missing energy and momentum might be produced. No limits on this possibility have been reported.

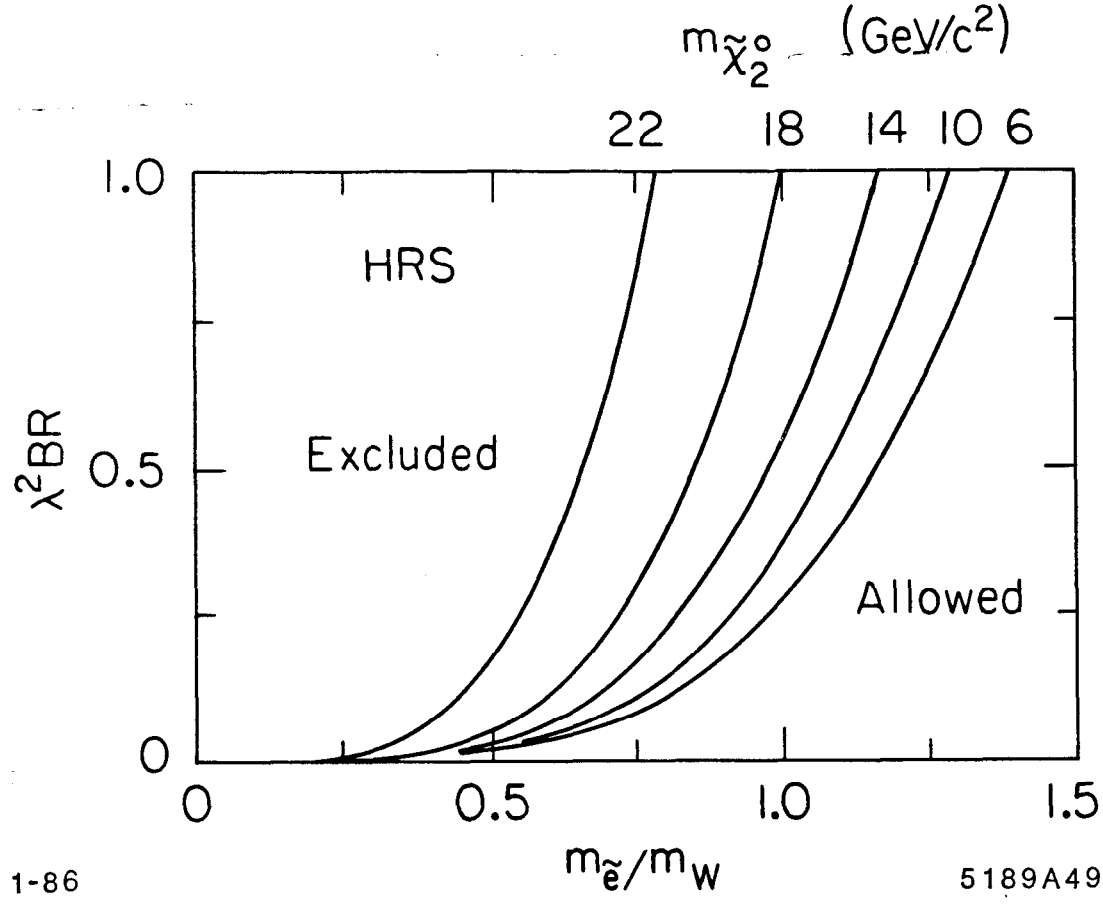

Figure 48. Limits on neutralino masses derived from limits on monojets in e^+e^- annihilation.

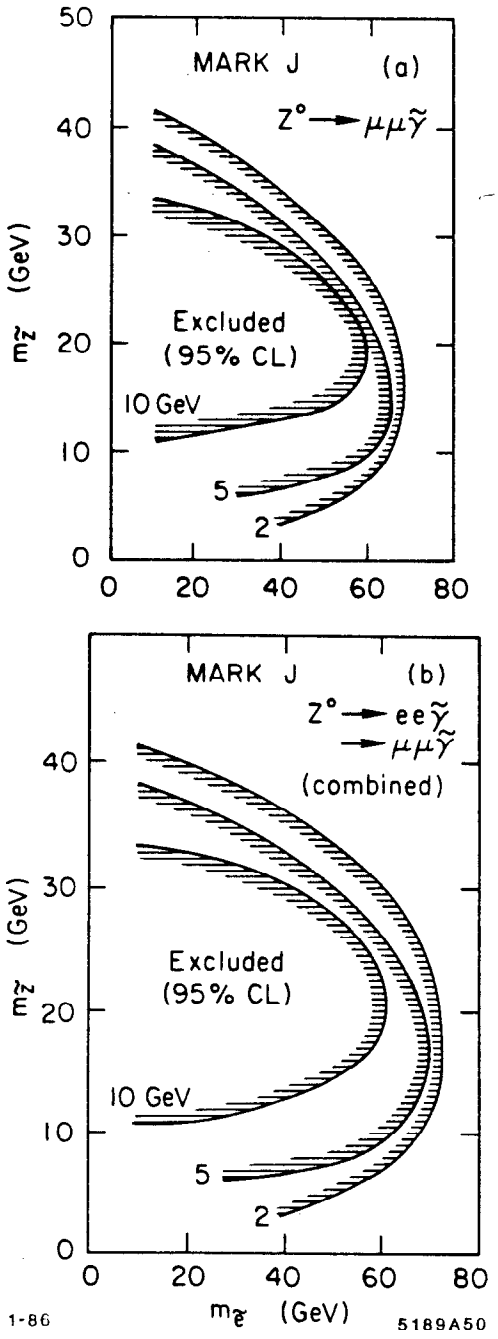

Figure 49. Limits on neutralino masses derived from a search for lepton pairs with missing energy and momentum.

IV. Searches for SUSY at Future e^+e^- Colliders

In this section we'll concentrate on the characteristics of the production of supersymmetric particles at beam energies near the Z^0 peak. We'll discuss several unique searches and measurements that can be made with e^+e^- beams. Evidence for new particle production through the weak current can appear indirectly as an unexpected shift in the mass of the Z^0 or increase in its width, or through observation of individual events (or samples of events) that contain these new states. The ability to polarize the initial electrons and positrons can provide useful tests of the couplings of these particles to the Z^0, and the measurement of $Z^0 \rightarrow \gamma\nu\bar{\nu}$ (the so-called "neutrino counting" experiment) will either discover evidence for supersymmetry or place important constraints on the possible masses of scalar neutrinos and neutralinos.

We remind ourselves that normal $R = +1$ fermions are arranged in left-handed weak isodoublets with third component of isospin $T_3 = \pm 1/2$, and right-handed singlets with $T_3 = 0$. The left and right-handed couplings to the weak neutral current are

$$g_L = T_{3L} - Q \sin^2 \theta_W \tag{50}$$

$$g_R = T_{3R} - Q \sin^2 \theta_W \quad . \tag{51}$$

The total width of the Z^0 is

$$\Gamma_z = \frac{G_F m_z^3}{12\sqrt{2}\pi} \sum (g_L^2 + g_R^2) \tag{52}$$

where the sum runs over all species that can contribute. The couplings of the $R = -1$ superpartners are prescribed by the Black Letter Law: they are identical to that of their $R = +1$ superpartners. So we have, for example,

$$g_L(\tilde{e}_L^-) = -\frac{1}{2} + \sin^2 \theta_W \tag{53}$$

and

$$g_R(\tilde{e}_R^-) = \sin^2\theta_W \quad . \tag{54}$$

This gives the ratio of partial widths,

$$\frac{\Gamma(Z^0 \to \tilde{\ell}_R^-\tilde{\ell}_R^+)}{\Gamma(Z^0 \to \ell^-\ell^+)} = \frac{g_R^2}{2(g_L^2+g_R^2)}\,\beta^3 \quad . \tag{55}$$

The factor of 1/2 in Eq. (55) arises from the spin algebra. If $\tilde{\ell}_L$ and $\tilde{\ell}_R$ are mass degenerate, and we sum over the two states, then

$$\frac{\Gamma(Z^0 \to \tilde{\ell}_L^+\tilde{\ell}_L^- + \tilde{\ell}_R^+\tilde{\ell}_R^-)}{\Gamma(Z^0 \to \ell^+\ell^-)} = \frac{1}{2}\beta^3 \quad . \tag{56}$$

Similar results hold for scalar quarks and neutrinos. A summary of the expected branching fractions for scalar leptons (degenerate masses are assumed when applicable) is given in Table V. The β^3 threshold factor, shown in Fig. 24, may not be negligible for masses near that of the Z^0.

Many of the event topologies and experimental techniques that result in signatures of supersymmetry at PEP and PETRA will continue to serve us well at the SLC and LEP. We'll not dwell at any length in this section on issues that are common to the two energy regimes.

A. Scalar Leptons

A glance at Table V will reveal that scalar leptons do not produce a large effect on the total width of the Z^0. Since we expect the mass of any scalar lepton to be greater than 20 GeV or so, then only $\sim$ 1% of all Z^0 decays will be to $\tilde{\ell}\bar{\tilde{\ell}}$. The accuracy with which Γ_{tot} can be determined is not known, but it would be fairly optimistic to expect less than $\sim$ 2% systematic uncertainty in the measurement.

Even with $BR(Z^0 \to \tilde{\ell}\bar{\tilde{\ell}}) \approx 1\%$, however, the direct observation of the acoplanar lepton pair left by the decay $\tilde{\ell} \to \ell\tilde{\gamma}$ (if it occurs) should be quite clear in data samples with $\gtrsim$ 1000 produced Z^0s. Radiative $Z^0 \to \gamma\ell^+\ell^-$ decays could

TABLE V

Branching fractions of the Z^0 into fermions and their supersymmetric partners.

Type	$\Gamma(R=+1)/\Gamma_{TOT}$	$\Gamma(R=-1)/\Gamma_{TOT}$
ν	6%	3% β^3
ℓ	3%	1.5% β^3
$q_{2/3}$	11%	5.5% β^3
$q_{1/3}$	14%	7% β^3

be a background in detectors that do not possess nearly complete solid-angle coverage with electromagnetic calorimetry, but notice that initial state radiation will not generate any sizable contamination. If a signal is observed, then it will be important to establish the Z^0 branching fraction and momentum and angular distributions of the final state leptons. These can all be used to determine whether or not the source is a scalar lepton. Of course, if the $\tilde{\ell}$ is stable, then it will appear as a massive charged particle that should be identifiable by TOF and/or dE/dx measurements.

B. Scalar Quarks

Scalar quarks with masses not too near the beam energy ($m_{\tilde{q}} \lesssim m_Z/4$) will be produced in $\sim 5\%$ of all Z^0 decays. This is a sizable contribution to the total Z^0 width. To establish the existence of a scalar quark, however, would require more direct evidence of its production. Light scalar quarks ($m_{\tilde{q}} \lesssim 10$ GeV/c^2) will produce final state jets that are collimated enough to allow the reconstruction of the production angle of the parent, but it will require a sufficiently large data sample to reveal the excess created near 90° by the $\sin^2\theta$ distribution of the scalar quark over the much larger background of normal quarks. Studies indicate[35] that, for masses larger than 10 GeV/c^2, it should be possible to isolate the decays of heavy quarks, or scalar quarks, by relatively simple cuts on the jet shape parameters that we've encountered before. A scalar quark can be distinguished from a normal sequential quark by measurement of the Z^0 partial width (Table V) and studies of possible leptonic decay modes. The leptonic decay rate of scalar quarks will depend upon masses and mixing parameters of gauginos.

C. Scalar Neutrinos

If there are three light scalar neutrino species, then their combined contribution to Γ_Z is quite large (Table V). As mentioned previously, the existence of a light $\tilde{\nu}$ may be visible in the neutrino-counting experiment described below. If the $\tilde{\nu}$ is stable, or has a significant decay branching fraction to $\nu\tilde{\gamma}$, then the neutrino-counting measurement will lead to an ambiguity between it and a fourth

generation $R = +1$ neutrino. Remember that

$$BR(Z^0 \to \nu_4\bar{\nu}_4) = 6\%\ \beta\ \text{(Dirac } \nu) \tag{57}$$

$$BR(Z^0 \to \nu_4\bar{\nu}_4) = 6\%\ \beta^3\ \text{(Majorana } \nu) \tag{58}$$

$$BR(Z^0 \to \tilde{\nu}\bar{\tilde{\nu}}) = 3\%\ \beta^3 \quad . \tag{59}$$

Furthermore, the probability that the parent particles in the final state are stable (or at least invisible) must be included to obtain proper estimates of the sizes of the contributions to the single photon data sample from Eqs. (57) – (59). It may not be possible to distinguish between these cases if the $\tilde{\nu}$ (or ν_4) has no visible decay modes.

The decays of massive scalar neutrinos into leptons and hadrons should be revealing. A fourth generation neutrino should decay to $\tilde{\ell}_1^-\tilde{\ell}_2^+\nu$ unless it simply doesn't mix with the lighter neutrino states. Leptonic decays of a scalar neutrino, on the other hand, are four-body final states, so the lepton spectrum will differ from that of the ν_4 decay. The most important parameter that can be estimated from leptonic and hadronic decays is clearly the mass of the parent particle. This combined with Eqs. (57) – (59) should allow the ambiguity to be resolved. With a large enough data sample it may also be possible to determine the production angle distribution of the parent, but this may be difficult if the mass is near the beam energy.

It should be noted that neutralino states $\tilde{\chi}_i^0$ can also counterfeit the signature of a scalar neutrino. In particular, the lightest $\tilde{\chi}_1^0$, if it is stable as we have assumed, will contribute to the neutrino-counting result an amount that depends on the size of its Higgsino component. The $\tilde{\chi}_i^0$ states are fermions, however, so if there are any leptonic or hadronic decay modes that can be isolated, then the production angle distribution can be measured, and will clearly separate it from a scalar neutrino. It's clear that detectors that possess large solid-angle electromagnetic and hadronic calorimetry or tracking will be needed to sort out the various decay modes of these new particles.

D. Gauginos and Higgsinos

The vector and axialvector coupling constants for several possible mixtures of gauge and Higgs fermions are given[36] in Table VI. For comparison g_v and g_a are also listed for a normal lepton. Notice that it is possible for one of the couplings to vanish. The branching fraction of the Z^0 into the chargino states is given by[37]

$$\frac{\Gamma(Z^0 \to \tilde{\chi}^+\tilde{\chi}^-)}{\Gamma(Z^0 \to \nu\bar{\nu})} = 4\beta F(m_{\tilde{\chi}},\ \theta_{mixing}) \tag{60}$$

where the function F can be as large as unity for some values of mixing angle and chargino mass. The production cross section for several cases is compared[38] with the μ-pair cross section in Fig. 50. Neutralinos have a similar form except that the production rate for identical fermions $\tilde{\chi}_i^0\tilde{\chi}_i^0$ contains a factor of 1/2 to account for Fermi statistics.

Some mixtures of chargino states result in Z^0 decay rates that are close to that expected for a heavy lepton $L^{\pm}$. If this is the case, then the absolute production rate cannot be used to distinguish between the two possibilities. The semileptonic decay modes illustrated in Fig. 51 provide probably the best discrimination. The three-body decay of a heavy lepton (Fig. 51a) is a purely $(V-A)$ interaction, while that of a heavy gaugino is an unknown combination of $(V-A)$ and $(V+A)$. The observed lepton momentum spectrum depends on this mixture as shown[39] in Fig. 52. In addition to perhaps signalling the production of the chargino state, this spectrum will also be an important indication of the nature of the mixing parameters that define the mass eigenstates. There also can be two-body decays (Fig. 51c) of a gaugino which are not present in the case of the heavy lepton. This signature will be quite clear, especially if there is more than one light scalar neutrino so that, for example, acoplanar $e-\mu$ events would appear with momenta spectra that differ from that expected for the tau.

—One of the more striking features of particle production at center of mass energies near the Z^0-pole is the strong forward-backward charge asymmetry created

TABLE VI

Some possible mixtures of gauge and Higgs fermions and their vector and axial vector weak couplings.

	State	g_v	g_a
Pure Higgsino	$\begin{pmatrix} \tilde{H}^-_{1L} \\ \tilde{H}^{+*}_{2R} \end{pmatrix}$	$-\frac{1}{2} + \sin^2\theta_W$	0
Pure Gaugino	$\begin{pmatrix} \widetilde{W}^-_L \\ \widetilde{W}^{+*}_R \end{pmatrix}$	$-1 + \sin^2\theta_W$	0
Mixtures	$\begin{pmatrix} \tilde{H}^-_{2L} \\ \widetilde{W}^{+*}_R \end{pmatrix}$	$-\frac{3}{4} - \sin^2\theta_W$	$-\frac{1}{4}$
	$\begin{pmatrix} \widetilde{W}^-_L \\ \tilde{H}^{+*}_{1R} \end{pmatrix}$	$-\frac{3}{4} + \sin^2\theta_W$	$+\frac{1}{4}$
Normal Lepton	L^-	$-\frac{1}{4} + \sin^2\theta_W$	$+\frac{1}{4}$

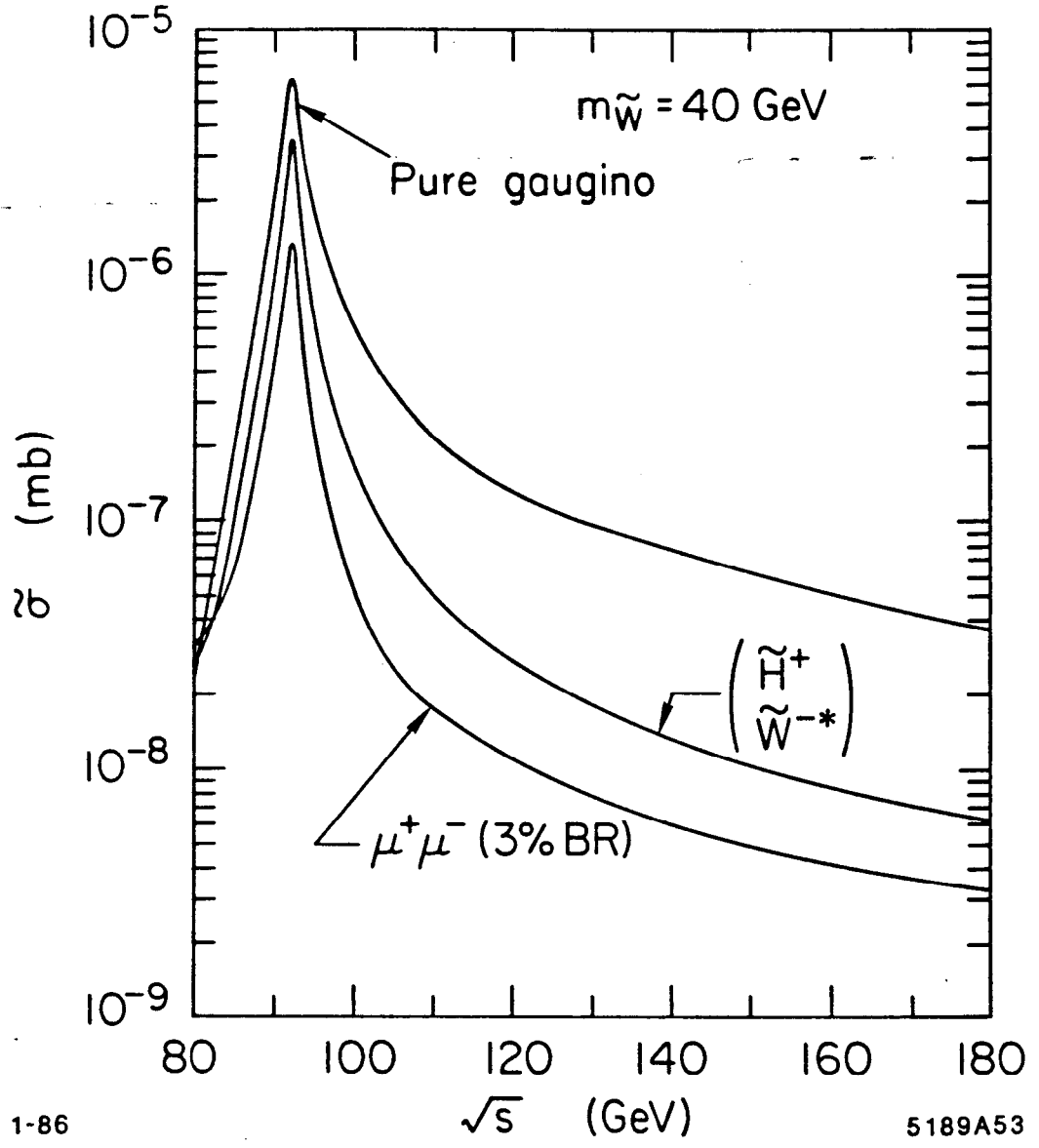

Figure 50. Production cross sections for gauginos and Higgsinos for different possible mass mixings. The μ-pair cross section is shown for reference.

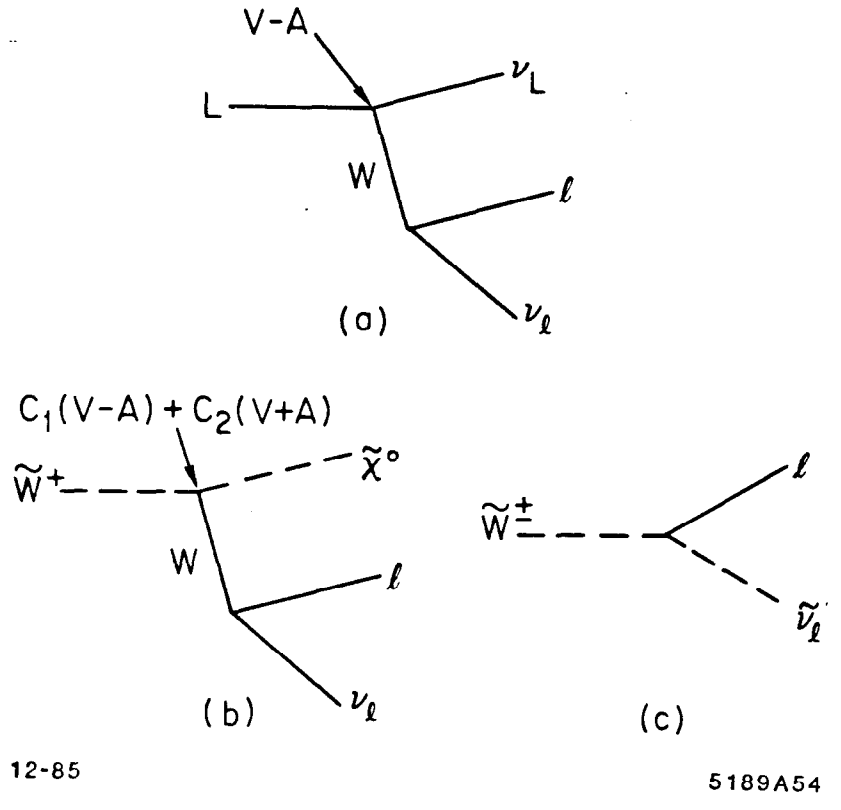

Figure 51. (a) The V–A weak decay of a heavy lepton. (b),(c) Decays of a supersymmetric gaugino.

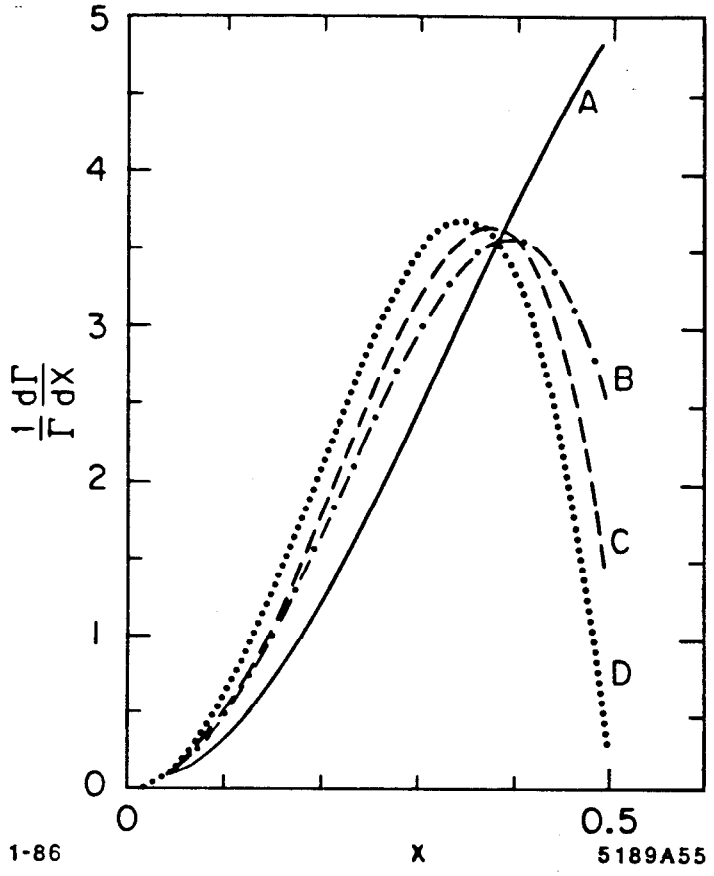

Figure 52. Lepton spectra produced by a pure V–A decay (A), and by decays with an increasing amount of a V+A interaction mixed into the V–A piece (B-D).

by the interference of the weak neutral current and the electromagnetic current. The differential cross section due to the graphs in Fig. 53a is[38]

$$\frac{d\sigma}{d\Omega} = \frac{3\alpha^2}{4s} \left[(1+A)(1+\cos^2\theta) + 2A'\cos\theta\right] \tag{61}$$

where A and A' are functions of the $\tilde{\chi}^{\pm}$ mass and A' is proportional to $8g_{a\tilde{\chi}}\,g_{ae}$. This is the cross section for the production of the $\tilde{\chi}^{\pm}$ relative to the direction of the initial $e^{\pm}$ as defined in Fig. 54. The asymmetry is determined by the axial vector coupling $g_{a\tilde{\chi}}$. The front-back charge asymmetry is defined by

$$A_{FB} = \frac{d\sigma(\theta) - d\sigma(\pi-\theta)}{d\sigma(\theta) + d\sigma(\pi-\theta)} = \frac{2\cos\theta}{1+\cos^2\theta}\,\frac{A'}{1+A} \quad . \tag{62}$$

In addition to the s-channel process in Fig. 53a, a chargino state may be produced through the t-channel exchange of a scalar electron neutrino as shown in Fig. 53b. Unless the mass of the $\tilde{\nu}_e$ is much larger than the mass of the $W^{\pm}$, then this graph will dominate the production of $\tilde{\chi}^{\pm}$ gaugino states. (The Higgsino coupling is suppressed by the electron mass.) The expected[36,38] forward-backward asymmetry for a variety of $\tilde{\chi}^{\pm}$ mixture is shown in Fig. 55. The same quantity is also plotted for μ-pairs. At first glance this would appear to provide a clean separation of chargino production from that of a heavy lepton, but there are several problems. Firstly, it will probably be necessary to use the leptonic decay modes to identify the parent particles (including their charges). These decays are perhaps 5–30% for a $\tilde{\chi}^{\pm}$, and the lower end of this range may be too small. Shown in Fig. 56b is a Monte Carlo generated[35] set of points that indicate how well the μ-pair asymmetry can be measured. Each of these points represents a month of continuous running at a machine luminosity of 10^{30} cm^{-2} sec^{-1}. The loss of another factor of 20 in signal size would have to be offset by an increase in luminosity. Perhaps more importantly, radiative corrrections drastically reduce[35] the size of the asymmetry (Fig. 56a). The reduction in the measured asymmetry is easily understood – even though the beam center of mass energy may be set

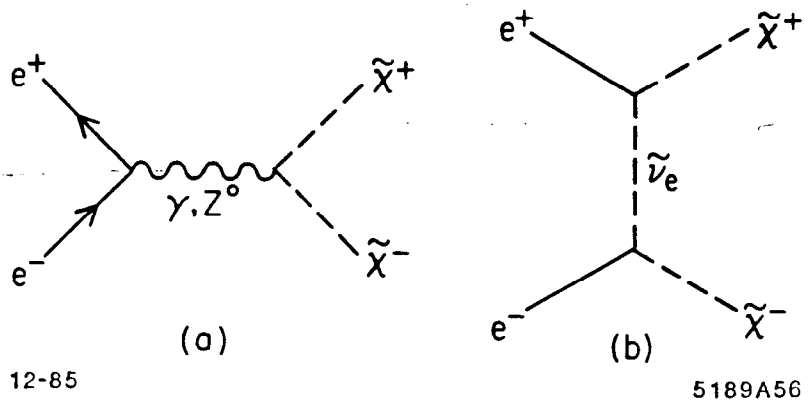

Figure 53. Pair production of chargino states.

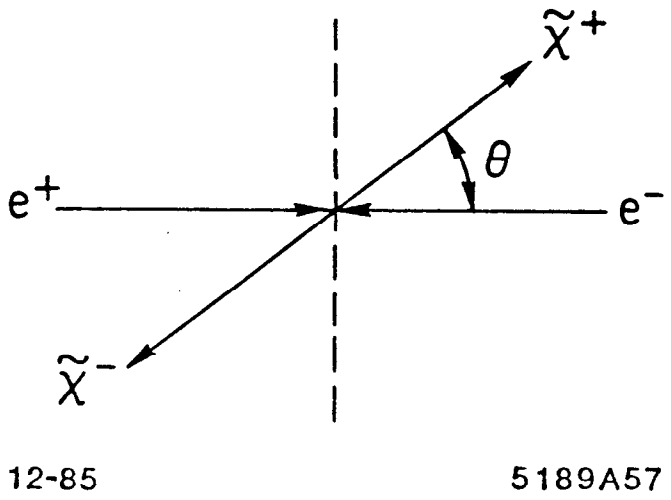

Figure 54. Polar angle of $\tilde{\chi}^+$ state with respect to e^+ direction.

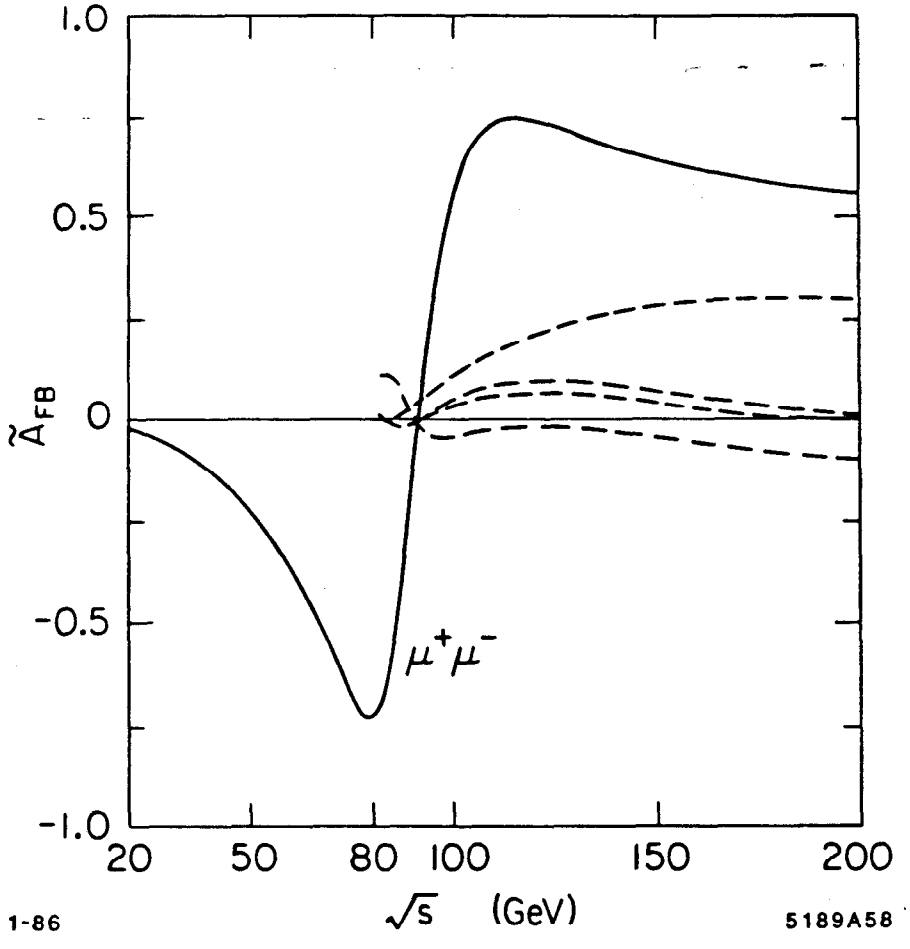

Figure 55. Expected forward-backward charge asymmetry for muon pairs produced at the Z^0 peak (solid curve), and for various mixtures of charged gaugino and Higgsino states (dashed curves). No radiative corrections have been made.

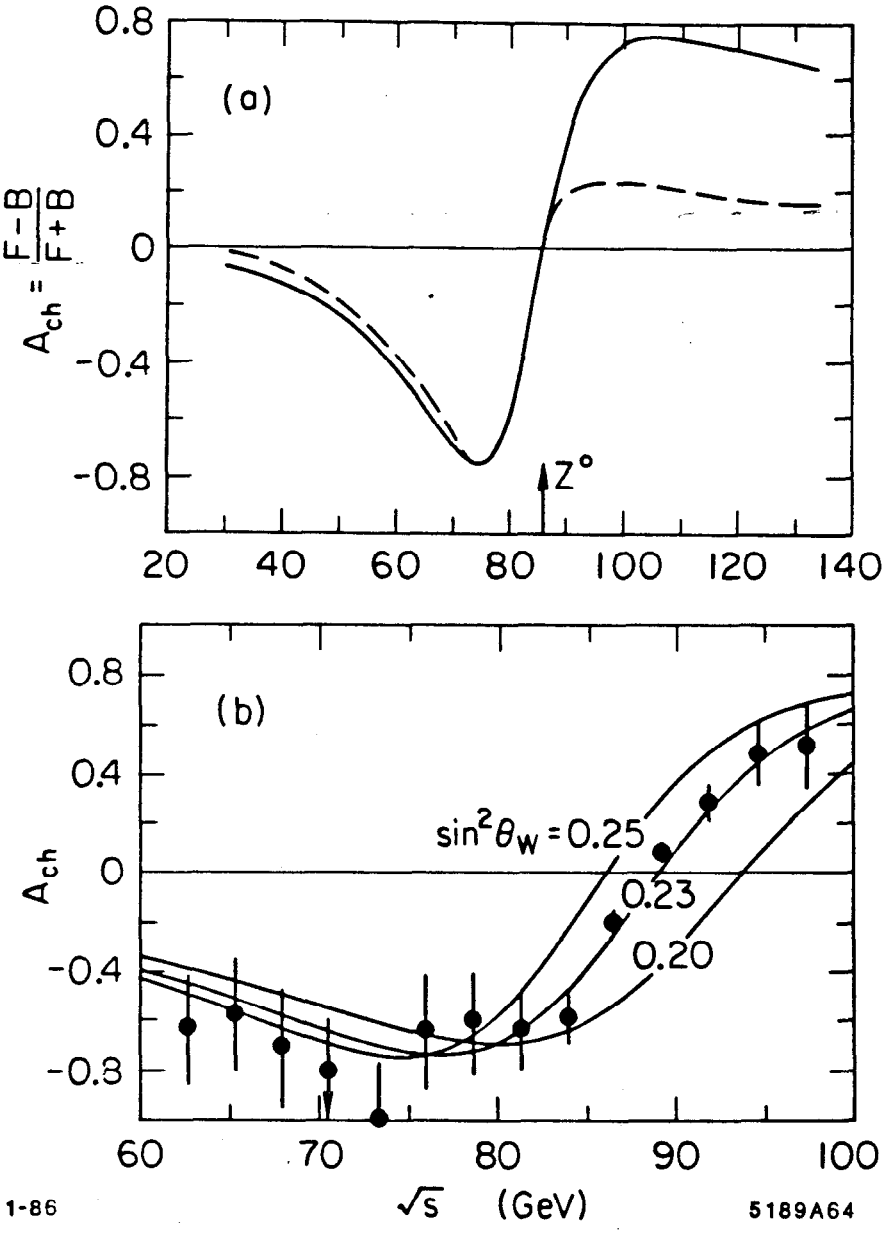

Figure 56. (a) μ-pair charge asymmetry without (solid line) and with (dashed line) radiative corrections. (b) Monte Carlo simulation of a measurement of the μ-pair charge asymmetry at the Z^0 peak.

above the mass of the Z^0, the product of the bremsstrahlung photon spectrum and the Z^0 Breit-Wigner is not small for a photon of just the right energy to place the reduced cms energy on the Z^0 peak. The asymmetry is smaller there, so the measured asymmetry is diminished. A glance back at Fig. 55 will show that much of the difference between the various curves will be eliminated by radiative corrections.

E. Polarization

One of the unique features of electron-positron machines is the ability to control the polarization of the initial state particles. In the case of the SLC the electron polarization is controlled at the e^- source by using circularly polarized light to excite a solid state cathode. This allows the longitudinal polarization to be quickly changed (pulse-to-pulse if necessary), and will create polarizations of 50–90%. LEP is a storage ring that can naturally produce transversely polarized electron and positron beams.

One of the most striking predictions[40] of supersymmetry is that the longitudinal asymmetry of a right-handed scalar lepton should be opposite in sign to that of a left-handed scalar lepton. Let's see how this comes about. Shown in Fig. 57 are two interfering diagrams that lead to the production of scalar muon pairs. The electromagnetic coupling (57a) is the same for $\tilde{\mu}_R$ and $\tilde{\mu}_L$. The coupling of the Z^0 is determined by g_L for the $\tilde{\mu}_L$ and by g_R for the $\tilde{\mu}_R$ state. As shown in the figure $g_R \approx -g_L = 1/4$. This means that the interference between the Z^0 piece and the electromagnetic piece will have opposite signs in the two cases! Since the Z^0 amplitude will depend upon the polarization of the electron beam, we can measure the magnitude of the change in the overall cross section as the spin of electron is flipped, and (for non-degenerate mass states) determine whether the final state particle is a $\tilde{\mu}_L$ or $\tilde{\mu}_R$. Define the longitudinal asymmetry,

$$A_{\parallel} = \frac{\frac{d\sigma}{d\Omega}\,(p_{\parallel} = +) - \frac{d\sigma}{d\Omega}\,(p_{\parallel} = -)}{\frac{d\sigma}{d\Omega}\,(p_{\parallel} = +) + \frac{d\sigma}{d\Omega}\,(p_{\parallel} = -)} \quad . \tag{63}$$

The expected longitudinal asymmetry for a 20 GeV $\tilde{\mu}$ is shown in Fig. 58 along

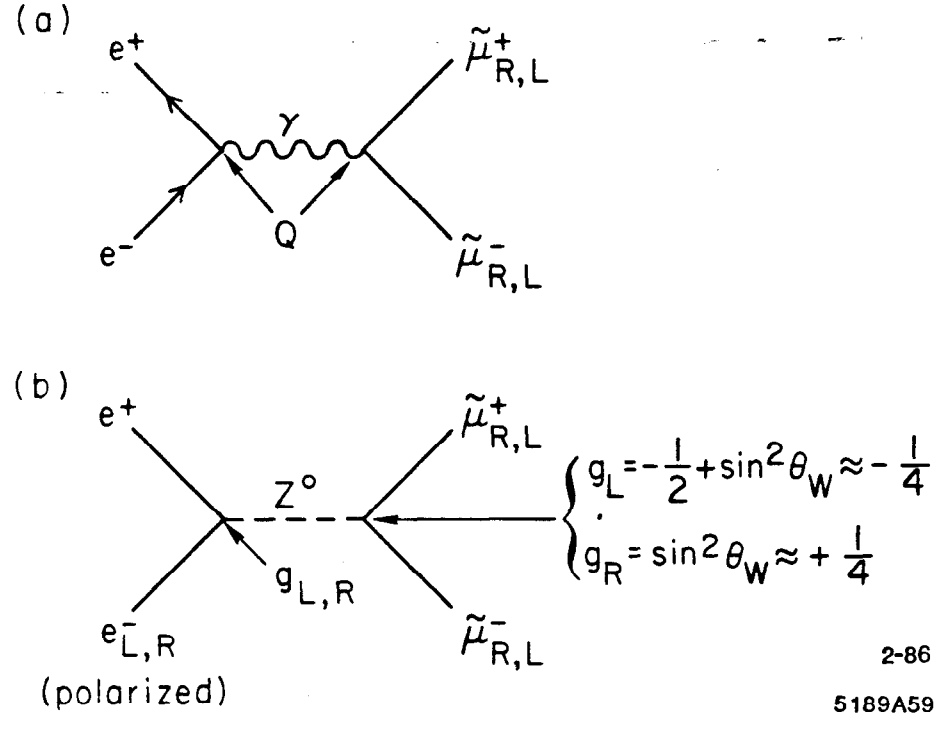

Figure 57. Schematic description of the factors that generate the longitudinal spin-flip asymmetry in e^+e^- annihilation near the Z^0 peak.

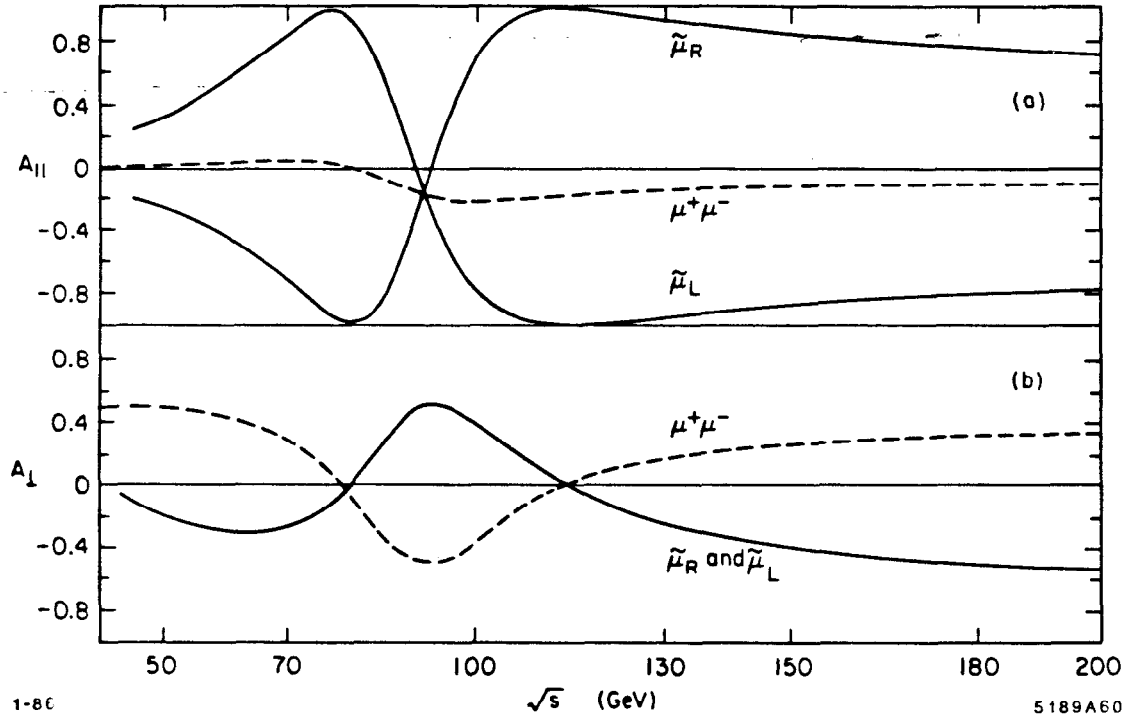

Figure 58. (a) Expected longitudinal asymmetry for $\tilde{\mu}_R$ and $\tilde{\mu}_L$ scalar muons. The same quantity for muons is plotted for reference. (b) Expected transverse asymmetry for $\tilde{\mu}_R$ and $\tilde{\mu}_L$.

with the same quantity for muons. If the $\tilde{\mu}_R$ and $\tilde{\mu}_L$ are mass degenerate, then the combined asymmetry will reduce to that of the muon. A parameter $A_\perp$ defined similarly to Eq. (63) can be defined for transversely polarized beams. Observation of this asymmetry in the production of scalar particles would be a beautiful signature of supersymmetry at work.

F. Mass and Width of the Z^0

The appearance of new $R = -1$ supersymmetric particles in decays of the Z^0 will modify both its mass and width. Fermion loop corrections to the Z^0 mass total about 5% for the known $R = +1$ particles, and they raise the expected mass from 88 GeV/c^2 to 93 GeV/c^2. If a light Higgsino exists then it can further shift the Z^0 mass, but most other $R = -1$ superpartners either do not contribute to the loop corrections or their effect is reduced by their masses. One calculation[41] of the effect of a light Higgsino yields a 500 MeV upward shift for $m_{\tilde{h}} \lesssim 10$ GeV/c^2, but the correction rapidly reduces to less than 200 MeV at larger $\tilde{h}$ masses. This is still large enough to ultimately be seen in measurements of $\sin^2\theta_W$, but it will require some additional evidence of the Higgsino to fully comprehend this effect.

We have already listed in Table V (and VI) the Z^0 partial decay widths of various supersymmetric particles. Here we discuss the contributions of supersymmetry to the "neutrino counting" reaction

$$e^+e^- \to \gamma + Z^0 \tag{64}$$

followed by the decay of the Z^0 into a final state that consists entirely of particles that interact only weakly in matter. We know of three neutrino generations that will create events of this type. The cross section produced by N_ν sequential light neutrino species is[42]

$$\frac{d^2\sigma}{dx\, d\cos\theta_\gamma} = \frac{G_F\alpha}{6\pi^2 x \sin^2\theta_\gamma} \cdot F_1(x,\, \cos\theta_\gamma) \cdot s \cdot \left\{ \frac{N_\nu(g_v^2 + g_a^2) + F_2(x, \cos\theta_\gamma)}{(1 - s(1-x)/m_z^2)^2 + \Gamma_z^2/m_z^2} + 2 \right\} . \tag{65}$$

In this formula $x = E_\gamma/E_b$, and F_1 and F_2 are not strongly dependent on x and $\cos\theta_\gamma$. This can be integrated with $N_\nu = 3$ and $M_z = 93$ GeV/c^2 to give the detected cross section shown[43] in Fig. 59. The cross section at $\sqrt{s} = m_Z$ corresponds to a Z^0 branching fraction of $\approx 1/4\%$. The photon line shape is shown in Fig. 60 for several center-of-mass energies. The difference in the signal provided by three families and that provided by four families is 25%, so a 3σ separation will require an 8% measurement of the cross section.

It is important to note, however, that the cross section for process (64) need not be given by Eq. (65) with N_ν equal to an integer. Even a standard sequential neutrino will contribute a fractional amount if its mass is not small and it doesn't mix with the lighter species. The relative contributions of stable neutrinos and scalar neutrinos are given by Eqs. (57) – (59). A light scalar neutrino will be produced in one half as many Z^0 decays as will a light standard sequential neutrino. Neutralinos will further increase the detected single photon cross section (Eq. 60). Almost any value up to the neutrino cross section (Eq. 65) is possible. A light Higgsino state would be produced quite prolifically in this channel.

The measurement of the cross section for the single photon process is a difficult one. An accurate normalization, either a luminosity measurement or a large and clean acceptance for muon-pairs, is required; the Z^0 line shape must be accurately known; and the detector resolution and acceptance must be optimized and well understood. It is particularly important to be able to reconstruct the origin of photon candidates in space (and time if possible) in order to reject and measure cosmic rays and machine related backgrounds. As a benchmark to the analysis, a 4σ discovery of a light scalar neutrino will require the measurement of the single photon production rate with an overall uncertainty of 3%.

V. Summary

The search for supersymmetry has so far yielded only negative results. The next generation of e^+e^- machines will be able to extend the hunt to masses that are $\sim 10^2$ GeV/c^2, but the role for which supersymmetry was invented demands

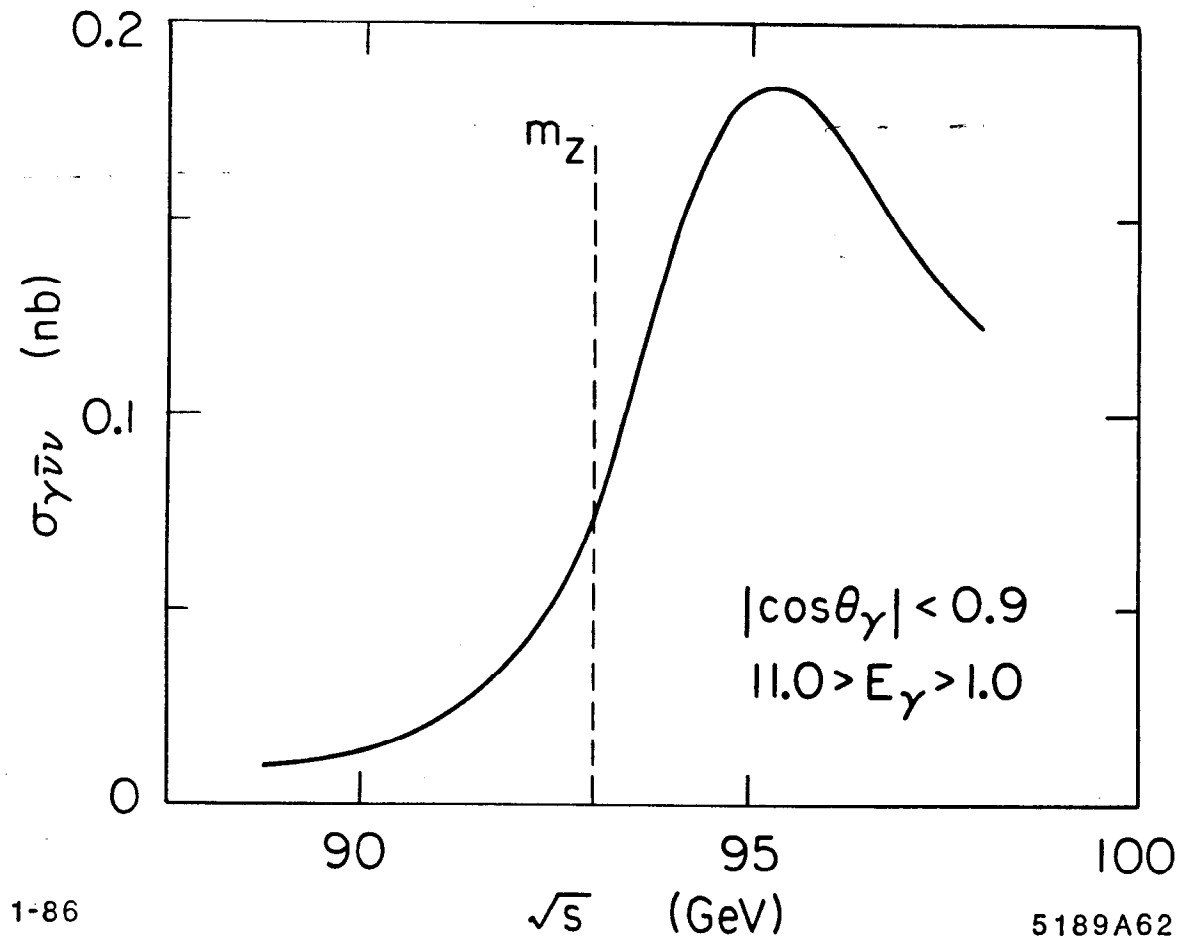

Figure 59. Visible cross section for single photons from the process $e^+e^- \to \gamma\nu\bar{\nu}$ with three neutrino flavors.

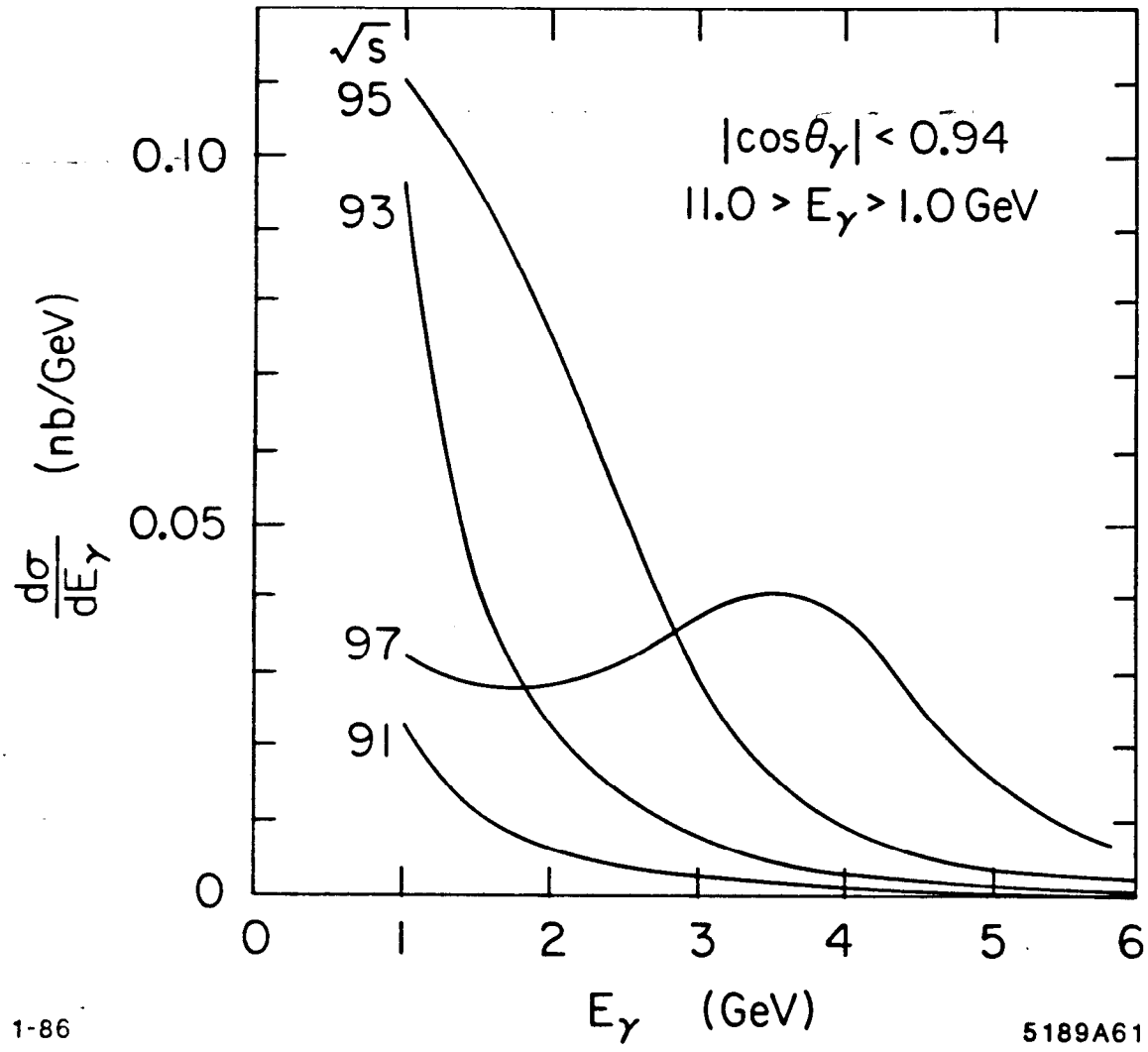

Figure 60. Spectrum of photons produced by the $e^+e^- \rightarrow \gamma\nu\bar{\nu}$ process at several center of mass energies.

only that it appear on a mass scale that is still an order of magnitude larger. Supersymmetry is likely to be with us for some time to come.

VI. Acknowledgments

The author would like to thank H. Haber for many enlightening discussions about the physics of supersymmetry.

References

1. Much of this and the next section are distilled from the reviews by H. E. Haber and G. L. Kane, Phys. Rep. 117, 76 (1985); and M. F. Sohnius, Phys. Rep. 128, 40 (1985).

2. P. Fayet, Phys. Lett. 86B, 272 (1979). G. L. Kane and J. P. Leveille, Phys. Lett. 112B, 227 (1982).

3. I. Hinchliffe and L. Littenberg, LBL 15022 (1982). Also published in Snowmass Summer Study, 242 (1982).

4. T. Kobayashi and M. Kuroda, Phys. Lett.134B, 271 (1984).

5. S. Komamiya, HD-PY 86/01 (1986).

6. R. Brandelik, *et al.*, TASSO Collaboration, Phys. Lett. 117B, 365 (1982). E. Fernandez, *et al.*, MAC Collaboration, Phys. Rev. D28, 2721 (1983).

7. W. Bartel, *et al.*, JADE Collaboration, Phys. Lett. 152B, 392 (1985).

8. D. Barber, *et al.*, MARK J Collaboration, Phys. Rev. Lett. 45, 1904 (1980).

9. L. Gladney, *et al.*, MARK II Collaboration, Phys. Rev. Lett. 51, 2253 (1983).

10. W. Bartel, *et al.*, JADE Collaboration, Phys. Lett. 152B, 385 (1985).

11. J. Ellis and J. S. Hagelin, Phys. Lett. 122B, 303 (1983).

12. N. Cabibbo, *et al.*, Phys. Lett. 105B, 155 (1981).

13. W. Bartel, *et al.*, JADE Collaboration, Phys. Lett. 139B, 327 (1984).

14. J. A. Grifols, X. Mor-Mur, and J. Sola, Phys. Lett. 114B, 35 (1982); P. Fayet, Phys. Lett. 117B, 460 (1982).

15. K. Grassie and P. N. Pandita, Phys. Rev. D30, 22 (1984).

16. R. J. Hollebeek, talk at this Summer School.

17. C. R. Nappi, Phys. Rev. D25, 84 (1982).

18. R. F. Schwitters, Proceedings of the XVIII International Conference on High Energy Physics, Tbilisi, Soviet Union, 1976, p. B34 (1977).

19. Summary completed by R. Zhu, CALT–68–1306, talk at DPF Meeting, Eugene, Oregon (1985).

20. W. Bartel, *et al.*, JADE Collaboration, Phys. Lett. 146B, 126 (1984).

21. M. Althoff, *et al.*, TASSO Collaboration, Z. Phys.C22, 307 (1984).

22. A. Chen, *et al.*, CLEO Collaboration, Phys. Rev. Lett. 52, 1084 (1984).

23. N. Lockyer, *et al.*, MARK II Collaboration, Phys. Rev. Lett. 51, 1316 (1983).

24. H. D. Dahmen, *et al.*, Nucl. Phys. B227, 291 (1983).

25. J. Zuk, G. C. Joshi, and J. W. G. Wignall, Phys. Rev. D28, 1706 (1983).

26. T. Goldman and H. Haber, Physica 15D, 181 (1985).

27. D. Besson, *et al.*, CLEO Collaboration, CLNS-85/701 (1985).

28. R. M. Barnett, H. E. Haber, and K. S. Lackner, Phys. Rev. D29, 1381 (1981).

29. H. E. Haber, R. M. Barnett, and K. S. Lackner, Phys. Rev.D29, 1990 (1984).

30. G. J. Feldman, *et al.*, MARK II Collaboration, Phys. Rev. Lett. 54, 2289 (1985).

31. G. L. Kane and W. B. Rolnick, Nucl. Phys. B232, 21 (1984).

32. E. Fernandez, *et al.*, MAC Collaboration, Phys. Rev. D31, 1537 (1985).

33. B. Adeva, *et al.*, MAC Collaboration, Phys. Rev. Lett. 53, 1806 (1984).

34. C. Akerlof, *et al.*, HRS Collaboration, Phys. Lett. 156B, 271 (1985).

35. Proceedings of the SLC Workshop on Experimental Use of the SLAC Linear Collider, SLAC-Rep-247 (1982).

36. J. M. Frere and G. L. Kane, Nucl. Phys. B223, 331 (1983).

37. B. Grinstein, J. Polchinski, and M. B. Wise, Phys. Lett. 130B, 285 (1983).

38. P. Chiappetta, *et al.*, Nucl. Phys. B262, 495 (1985).

39. T. Fukai, *et al.*, WU-HEP-85-3 (1985).

40. P. Chiappetta, *et al.*, Nucl. Phys. B259, 365 (1985).

41. J. A. Grifols and J. Sola, Phys. Lett. 137B, 257 (1984).

42. E. Ma and J. Okada, Phys. Rev. Lett. 41, 287 (1978).
G. Barbiellini, B. Richter, and J. L. Siegrist, Phys. Lett. 106B, 414 (1981).

43. R. Thun, private communication.